

THE STELLAR ARCHEOLOGY OF THE M33 DISK: RECENT STAR-FORMING HISTORY AND CONSTRAINTS ON THE TIMING OF AN INTERACTION WITH M31 ^{1 2}

T. J. Davidge, & T. H. Puzia ³

*Herzberg Institute of Astrophysics,
National Research Council of Canada, 5071 West Saanich Road,
Victoria, BC Canada V9E 2E7
email: tim.davidge@nrc.ca, tpuzia@gmail.com*

ABSTRACT

Images recorded with MegaCam are used to investigate the recent ($t \leq 0.25$ Gyr) star-forming history (SFH) of the Local Group Sc galaxy M33. The data sample the entire star-forming disk, as well as areas immediately to the north and south of the galaxy. The properties of the stellar disk change near $R_{GC} = 8$ kpc. Within this radius the luminosity function of main sequence stars indicates that the star formation rate (SFR) has been constant with time during at least the past 250 Myr, while at larger radii the SFR has declined during this same time period. That the recent SFR in the inner disk has been constant suggests that M33 has evolved in isolation for at least the past ~ 0.5 Gyr, thereby providing a constraint on the timing of any recent interaction with M31. The color of the main sequence ridgeline changes with radius, suggesting a gradient in extinction of size $\Delta A_V / \Delta R_{GC} = -0.05$ magnitudes kpc^{-1} . The fractional contribution that young stars make to the total mass of the stellar disk changes with radius, peaking near 8 kpc. Evidence is also presented of systematic spatial variations in the SFH of the disk, such that the SFR during the past 100 Myr in the southern half of the galaxy has been ~ 0.4 dex higher than in the northern half. Finally,

¹Based on observations obtained with MegaPrime/MegaCam, a joint project of CFHT and CEA/DAPNIA, at the Canada-France-Hawaii Telescope (CFHT) which is operated by the National Research Council (NRC) of Canada, the Institut National des Science de l'Univers of the Centre National de la Recherche Scientifique (CNRS) of France, and the University of Hawaii.

²This research used the facilities of the Canadian Astronomical Data Center, operated by the National Research Council of Canada with the support of the Canadian Space Agency.

³Present Address: Department of Astronomy and Astrophysics, Pontificia Universidad Catolica, Santiago, Chile 7820436

structures with sizes spanning many kpc that contain blue objects – presumably main sequence stars that formed during intermediate epochs – are identified near the disk boundary. It is argued that these are tidal features that were pulled from the main body of M33 and – in some cases – are the fossil remnants of star formation that occurred in an extended disk during intermediate epochs.

Subject headings: galaxies: evolution — galaxies: spiral — galaxies: individual(M33)

1. INTRODUCTION

The largest members of the Local Group have not evolved passively, but have experienced interactions that are consistent with hierarchical assembly. Perhaps the most overt signatures of this activity in the Local Group are the stellar streams that have been detected in the outer regions of M31 (e.g. Ibata et al. 2007; Tanaka et al. 2010). The location and morphology of the Sagittarius dwarf galaxy (Ibata et al. 1994), coupled with the presence of coherent streams in the Galactic disk (e.g. Helmi et al. 2006) and globular clusters that follow an age-metallicity relation that is distinct from that defined by the majority of Galactic globular clusters (e.g. Forbes & Bridges 2010), indicate that the Galaxy also has not evolved in isolation. There is evidence that the effects of recent interactions on the properties of the Galactic disk have not been as great as they have been on the M31 disk (e.g. Hammer et al. 2007).

As the nearest Sc galaxy, M33 is on a par with the LMC in serving as a benchmark for understanding the stellar content and evolution of late-type galaxies. However, during the past few years, evidence has been presented that M33 and M31 may have interacted during cosmologically recent epochs, and such an interaction may have affected the properties of the M33 disk. Braun & Thilker (2004) find an HI structure that appears to link M33 and M31, and Bekki (2008) models this as a tidal bridge that formed during an interaction 4 – 8 Gyr in the past. Putman et al. (2009) investigate the possible orbital trajectories of M31 and M33 as constrained by their present-day locations and radial velocities. They conclude that at some point during the past $\sim 1 - 3$ Gyr the tidal radius of M33 may have been ≤ 15 kpc due to an encounter with M31, which would have greatly affected the disk of M33. Simulations discussed by McConnachie et al. (2009) also support the notion of an interaction between M31 and M33 that may have disturbed the M33 disk. Their simulations suggest that the pericentric separation ~ 2.5 Gyr in the past may have been as small as 40 kpc.

The spatial distribution and kinematic properties of the interstellar medium (ISM)

of M33 show signatures of a recent tidal interaction. The HI in the outer regions of M33 has an S-shaped morphology and is distributed over $28 \times 38 \text{ kpc}^2$, with almost one fifth of the gas by mass located outside of the star-forming disk (Putman et al. 2009). While S-shaped structures are classical signatures of tidal interactions in simulations (e.g. Barnes & Hernquist 1992), the arms of the HI emission associated with M33 are in the opposite direction of disk rotation, possibly suggesting an encounter in the opposite direction of M33 disk rotation.

The HI in M33 also has a high velocity dispersion when compared with other late-type galaxies, with a mean $\sigma = 18.5 \text{ km sec}^{-1}$ (Putman et al. 2009). While high velocity dispersions in the outer regions of disks are not uncommon, and have been interpreted as the product of heating by halo sub-structures (e.g. Herrmann et al. 2009), the entire gas disk of M33 is kinematically hot. Block et al. (2007) argue that the warp in the ISM at 5 kpc could result from the accretion of gas with an angular momentum vector that was distinct from that of the main body of the disk, which might be expected to occur due to an interaction. Finally, while molecular clouds in M33 have some characteristics that are similar to their counterparts in the Milky-Way and M31 (Sheth et al. 2008), the ratio of atomic to molecular gas in M33 is high, and the fraction of molecular gas in giant molecular clouds is low when compared with the Galaxy (Verley et al. 2010). Both of these properties are consistent with a disturbed ISM.

1.1. Stars and Gas in M33: A Brief Review

Stars and gas in M33 provide a fossil record of the events that shaped its past. Because of the obvious challenges presented by crowding, much of the previous work on the resolved stellar content of M33 has examined the outer regions of the disk. There are hints that the orbits of disk stars in M33 may have been disrupted, such that the radial age distribution differs from that in more isolated late-type spirals (Gogarten et al. 2010). In fact, it has been known for some time that stars with properties that are consistent with a disk origin appear at large radii in M33, as might be expected if the disk was disrupted. Davidge (2003) found that red giant branch (RGB) stars located between 14 and 17 kpc (7 – 9 disk scale lengths) from the center of M33 have $[M/H] \sim -1 \pm 0.3 \text{ dex}$. This metallicity is higher than expected for stars that belong to a classical metal-poor halo, but is within the range expected for disk objects. A similar situation occurs in M31, where moderately metal-rich stars are distributed throughout much of the outer regions of the galaxy (e.g. Bellazzini et al. 2003).

Davidge (2003), Block et al. (2007) and Verley et al. (2009) find evidence of a large

population of C stars in the outer disk of M33. The discovery of a large number of C stars is suggestive of an elevated star formation rate (SFR) 1 – 3 Gyr in the past, which is the likely time of an interaction with M31 (Putman et al. 2009). There are indications that these stars may belong to a population that is distinct from the inner disk population. Indeed, if – as argued by Block et al (2007) – the change that is seen in the $8\mu\text{m}$ profile is driven by the circumstellar dust contents of M giants and C stars, then this is indicative of a change in stellar content. Block et al. (2007) further suggest that the formation of the C stars may be tied to the events that caused the warp in the M33 HI disk at $R_{GC} = 5$ kpc.

Barker & Sarajedini (2008) explore the chemical evolution of the outer regions of M33. The chemical evolution deduced from CMD morphology does not follow that expected for a closed box; rather, a time-variable rate of infall is required to explain the enrichment history. Barker & Sarajedini (2008) find that the peak rate of gas accretion occurred 3 – 7 Gyr in the past, during which time 50 – 60% of all gas that has fallen onto the disk was accreted. The rate of infall has since plunged, with only 10% of all infalling gas being accreted during the past 3 Gyr. While Barker & Sarajedini (2008) discuss these results in the context of protracted disk assembly, the drop in the infall rate some 3 Gyr in the past coincides with the timing of an interaction between M31 and M33 as predicted by both Putman et al. (2009) and Bekki (2008). A modest infall rate at the present day would be expected if circumgalactic gas was stripped by an encounter with another galaxy.

Past studies have found evidence for systematic radial variations in the star-forming history (SFH) of the M33 disk. Bastian et al. (2007) find that the number of young stellar groups drops suddenly at radii > 4 kpc, which they attribute to a change in the star-forming ISM, and it is only in the central 4 kpc that Park et al. (2009) find clusters with $\log(t) \leq 7.8$. The impact of systematic gradients in the SFH are also seen in integrated light. This is demonstrated by Munoz-Mateos et al. (2007), who find a radial gradient in the specific SFR (sSFR) of M33 based on measurements in the UV and IR.

Cioni et al. (2008) examine the distribution of M giants and C stars in M33, and find that the C/M ratio peaks ~ 35 arcmin (~ 10 kpc) from the galaxy center. The radial variation in C/M is likely a product of gradients in both mean metallicity and age, in the sense that younger mean ages and higher metallicities occur at smaller radii. Using C/M as a metallicity indicator, Cioni (2009) finds a progressive radial decrease in metallicity with increasing radius in M33 out to 8 kpc, while at larger radii the metallicity profile is flat. Cioni (2009) interprets the break in the metallicity profile as an interface between inner and outer disk/halo components.

The spectral energy distribution of the M33 disk at visible wavelengths is consistent with insight-out formation (Li et al. 2004), although the radial age distribution of stars may

be affected by processes other than the mechanics of disk assembly. Williams et al. (2009) use deep ACS images to examine stellar content over a range of radii in M33. They find that mean age drops as radius increases when $R < 8$ kpc, but at $R > 8$ kpc mean age increases with radius. Such a radial age inversion is consistent with simulations of disk evolution (e.g. Roskar et al. 2008; Sanchez-Blazquez et al. 2009), and can be understood in the context of inside-out disk formation coupled with the dynamical evolution of disk stars, which causes the outermost regions of the disk to be populated by stars that formed at smaller radii, but have migrated outwards. The most overt signature of such processes at work in M33 is the difference in scale lengths that characterize the distributions of young stars and old stars, in the sense that old stars are distributed over larger spatial scales than young stars (e.g. Verley et al. 2009; Davidge et al. 2011).

Metallicity gradients are a natural consequence of disk assembly in a hierarchical universe (e.g. Colavitti et al. 2009). However, if M31 passed close to M33 then tidal forces may have mixed gas throughout the disk, thereby flattening pre-existing gradients in the ISM. Rosolowsky & Simon (2008) examine the emission spectra of HII regions that span a range of radii in M33 and find that $\Delta[\text{O}/\text{H}]/\Delta R \sim -0.027 \pm 0.012$. This is substantially smaller than the mean $[\text{O}/\text{H}]$ gradient in the 39 disk galaxies studied by Zaritsky et al. (1994), for which $\langle \Delta[\text{O}/\text{H}]/\Delta R \rangle = -0.058 \pm 0.009$, where the uncertainty is the standard error in the mean. A caveat is that giant HII regions, upon which many of the measurements in the Zaritsky et al. (1994) compilation are based, may define steeper gradients than those computed from all HII regions, regardless of size (Magrini et al. 2010).

Rosolowsky & Simon (2008) find considerable scatter about the mean relation between $[\text{O}/\text{H}]$ and radius in M33, which they attribute to local inhomogeneities in the ISM. An intriguing result is that HII regions with low $[\text{O}/\text{H}]$ (and hence presumably low total metallicity) are found at small radii, suggesting that material that has undergone only modest amounts of chemical enrichment is present in the part of M33 that is expected to be the most chemically mature. The presence of such material could be due to the tidally-induced mixing of gas from the outer regions into the central regions of the galaxy. Alternatively, Magrini et al. (2010) argue that the comparatively low mean metallicity computed for HII regions in the central kpc of M33 may be a result of selection effects in surveys that require the detection of $[\text{OIII}]\lambda 4363$, which is a diagnostic of electron temperature. Still, it is evident from their Figure 19 that the mean $[\text{O}/\text{H}]$ in the central kpc remains lower than that at 1.5 kpc even if HII regions that do not have $[\text{OIII}]\lambda 4363$ detections are included in the sample.

Very young stars might be expected to track the metallicity trends defined by HII regions. However, blue supergiants (BSGs) in M33 define a steeper radial metallicity gradient than HII regions (U et al. 2009), with a slope that is consistent with the mean in the Zaritsky

et al. (1994) HII sample. A possible explanation for this difference in gradients is that U et al. (2009) do not find stellar counterparts to the oxygen-poor HII regions detected at small radii by Rosolowsky & Simon (2008); this may be a consequence of the modest number of BSGs studied.

The ages of HII regions and PNe differ by at least a few hundred Myrs, and so insights into the recent chemical enrichment history of the M33 disk can be obtained by comparing abundance gradients deduced from these types of nebulae. Magrini et al. (2009) find that $\Delta[\text{O}/\text{H}]/\Delta R = -0.031 \pm 0.013$ amongst M33 PNe, and this agrees with the gradient measured from HII regions by Rosolowsky & Simon (2008). Metallicity gradients are expected to steepen with time if there is infall, and Magrini et al. (2009) attribute the lack of evolution of the $[\text{O}/\text{H}]$ gradient to a low accretion rate during the past few Gyr. Such a drop in infall rate during intermediate epochs is in broad agreement with the conclusion reached by Barker & Sarajedini (2008) from an investigation of CMDs. Alternatively, a static abundance gradient with time could also signal the accretion of gas with low or modest amounts of enrichment, at a fortuitous rate that is sufficient to balance any increase in metallicity that may arise from the recycling of nuclear processed material into the ISM.

Some properties of M33 may not be typical of late-type spiral galaxies in general. For example, when compared with other late-type galaxies, the star-forming activity in M33 appears to be subdued. Indeed, while the sSFR of M33 is close to the midpoint of spiral galaxies in general, it is near the low end of galaxies of similar morphological type (Munoz-Mateos et al. 2007). The radial sSFR gradient in M33 is also steeper than in the majority of galaxies (Munoz-Mateos et al. 2007). This may indicate a low sSFR at small radii, although the circumnuclear stellar content of M33 is similar to that in other nearby late-type spirals (Davidge 2000; Davidge & Courteau 2002).

The gas within 8 kpc of the center of M33 appears to have a sub-critical density for triggering star formation (Martin & Kennicutt 2001), and this is one possible explanation for the low sSFR when compared with other late-type spirals. Considering the low gas density, the chemical properties of M33 are suggestive of a star-forming efficiency (SFE) that is higher than that among other nearby galaxies, and the SFE increases to progressively larger radii (Magrini et al. 2010). That star-forming activity occurs on a large scale in an environment with a low density may be related to the shear rate (Martin & Kennicutt 2001), which influences the frequency of collisions between molecular clouds, or an increase in ISM pressure caused by material falling into the galaxy, coupled with a kinematically hot interstellar environment (Putman et al 2009). The gravitational field of stars in the disk may also facilitate the collapse of star-forming material (e.g. Verley et al. 2010).

1.2. The Current Study

The youngest stars in late-type galaxies play a key role in defining the classical morphological characteristics of these systems, and if M33 has experienced a recent interaction then residual signatures of such an event may be evident in the spatial distribution of these objects. Massive young stars are also brighter than the vast majority of older stars, and so are less prone to crowding in ground-based observations. In the present paper, u^* and g' images obtained with MegaCam on the 3.6 metre Canada-France-Hawaii Telescope (CFHT) are used to investigate the properties of young stars in M33.

Two specific aspects of young stars in M33 are examined in this paper. First, we investigate the recent SFH of the M33 disk, with emphasis on how it has changed with time and location during the past few 100 Myr. There are considerable uncertainties associated with SFHs that are based on integrated light indicators, and these uncertainties are avoided by employing star counts as a probe of SFH. While area-to-area variations in SFR may occur within a galaxy due to the passage of spiral density waves or stochastic effects, when averaged over long timescales and large areas the SFRs of isolated star-forming disks are expected to be more-or-less constant with time. Aside from dense galaxy clusters, where there may be a high-density ambient intergalactic medium, galaxy-wide departures from a constant SFR in intermediate mass galaxies are likely triggered by tidal encounters.

Second, we search for young or intermediate age stars outside of the main body of the M33 disk. One might expect a mixed bag of such objects at large distances from the galaxy center. The outermost regions of the stellar disk may contain stars that migrated from smaller radii (e.g. Sellwood & Binney 2002), while the passage of spiral density waves might generate isolated areas of star formation (Bush et al. 2010). Tidal effects may pull gas from the inner regions of disks, and studies of interacting galaxies indicate that star formation is not uncommon in tidal debris fields (e.g. Neff et al. 2005). Tidal interactions can also redistribute existing stars over large areas (e.g. Teyssier et al. 2009). If a tidal plume formed due to an interaction between M31 and M33 then young/intermediate age stars, that either were present in the disk prior to the interaction or formed during the interaction, might be found in the circumgalactic environment.

An important aspect of this study is the near-complete spatial coverage of the M33 disk. The only areas missed in the stellar disk are those that fall in the gaps between detector banks. While crowding is an issue within 2 kpc of the galaxy center, a large fraction of the brightest blue stars are still resolved there with these data (§6). Such complete areal coverage facilitates the suppression of stochastic variations in the SFH that may occur over kpc spatial scales. In this sense, the SFH deduced from our data is more akin to what might be derived from – say – fiber spectroscopic studies of distant galaxies, rather than from pencil-beam

surveys of distinct areas within nearby galaxies that typically cover only a few kpc².

Observations in u^* are another important aspect of this program. The u^* filter is well-suited to investigations of intrinsically luminous main sequence stars, not only because they have effective temperatures that places the peak of their spectral energy distributions shortward of $0.4\mu\text{m}$, but also because of the enhanced contrast with respect to the (predominantly red) unresolved stellar body of M33 when compared with filters having longer central wavelengths. Observations in u^* are also beneficial when searching for diffuse ensembles of young and intermediate age stars in the outermost regions of the disk, where the fractional contamination from unresolved background galaxies, the majority of which have red colors (e.g. Davidge 2008; Mouhcine & Ibata 2009), is substantial. An obvious downside to observing in u^* is that there is increased sensitivity to reddening variations when compared with filters that have longer effective wavelengths.

The distance modulus computed by Bonanos et al. (2006), $\mu_0 = 24.92$, is adopted for this study. This distance estimate is based on a geometric calibration (the orbital properties of stars in an eclipsing binary), and is in excellent agreement with recent distances computed from the properties of B supergiants and ACS-based observations of the RGB-tip (U et al. 2009). Galleti et al. (2004) compare various distance moduli of M33, and the results are summarized in their Figure 10. While the Bonanos et al. (2006) value is near the upper end of the distance estimates considered by Galleti et al. (2004), it still falls well within the scatter envelope. In any event, the basic results of this study will not change greatly if a distance modulus that is – say – 0.2 mag smaller were to be adopted.

The line-of-sight extinction is assumed to originate in a uniform absorbing sheet in front of M33, and the adopted total extinction is the result of combining estimates of the foreground and internal components. The foreground component is taken from Schlegel et al. (1998), for which $A_B = 0.18$, while the internal component is that computed for M33 by Pierce & Tully (1992), for which $A_B = 0.16$; thus, the total extinction is $A_B = 0.34$ magnitudes. In §4 it is demonstrated that this model correctly predicts the mean extinction towards main sequence stars in M33. Still, it should be kept in mind that dust in M33 is not uniformly distributed. U et al. (2009) find that line-of-sight dust extinctions among bright A and B supergiants vary by ~ 0.16 magnitude in $(B - V)$, with a mean $E(B - V) = 0.08$. This mean is consistent with the combined foreground and internal reddening values used here. It is demonstrated in §4 that reddening variations, as gauged by the width of the main sequence, are not substantial, with $\Delta E(B - V) \leq \pm 0.1 - 0.2$ throughout much of the M33 disk.

The paper is structured as follows. Details of the observations and the photometric measurements are discussed in §2 and §3. The color-magnitude diagrams (CMDs) of stars

and an assessment of reddening variations throughout the disk are presented in §4. The recent SFH throughout the disk is investigated in §5 by comparing the luminosity function (LF) of main sequence stars with models. The spatial distribution of young and intermediate age stars throughout the disk and its immediate surroundings is examined in §6. A summary and discussion of the results follows in §7.

2. OBSERVATIONS & REDUCTIONS

This study uses a mix of archival and newly recorded MegaCam images. MegaCam (Boulade et al. 2003) is the wide-field $0.35 - 1.1\mu\text{m}$ imager on the 3.6 meter Canada-France-Hawaii Telescope (CFHT). The detector is a mosaic of thirty six 2048×4612 pixel E2V CCDs that are deployed in a 4×9 format. A single exposure covers $\sim 1 \times 1$ degree² with 0.18 arcsec pixel⁻¹ sampling.

The locations of the five fields that are discussed in this paper are indicated in Figure 1. The data for the Center Field consists of archival u^* and g' images that were recorded as parts of programs 2003BF15, 2004BH06, 2004BH20, and 2004BF26. The majority of the exposures recorded for these programs have similar integration times, lunar phasing, and (sub-arcsec) image quality; hence, they form a homogeneous dataset.

The archival data were downloaded from the CFHT archive hosted by the Canadian Astronomical Data Center (CADC), and were screened to remove exposures recorded during times of poor seeing, poor transparency, and/or bright lunar phase. A catalogue of the exposures that were retained for this program is provided in Table 1. Stars in the final combined images of the M33 Center Field have FWHM ~ 0.9 arcsec in both filters.

The four other MegaCam pointings were recorded during semester 2009B, and these sample the northern and southern edges of the M33 disk. The fields overlap, allowing the field-to-field consistency of the photometric calibration to be checked, while also providing an empirical estimate of random errors in the photometry. Five 150 sec exposures were recorded per field in g' , and ten 440 sec exposures were recorded in u^* . The data were recorded during grey time (i.e. partial lunar phase) to permit scheduling flexibility. A linear 5 point dither pattern was employed to facilitate the suppression of bad pixels and cosmic rays. Stars in the final combined images have FWHM ~ 0.9 arcsec in both filters.

Initial processing of the data, which included bias removal and flat-fielding, was done with the CFHT ELIXER pipeline. To provide images of a tractable size for photometric measurements and to better monitor point spread function (PSF) variations across the wide MegaCam field, sub-mosaics of CCDs in 2×3 groups were constructed for subsequent pro-

cessing – each 4×9 MegaCam CCD mosaic was thus divided into $2 \times 3 = 6$ sub-mosaics. There are wavelength-dependent distortions that introduce offsets of a few pixels between the u^* and g' images near the edge of the MegaCam field. These offsets were removed by using the GEOMAP/GEOTRAN tasks in IRAF to map the u^* images into the g' reference frame. The final processing steps were to stack and combine the sub-mosaic images, and then trim the results to the area of common exposure time.

3. PHOTOMETRIC MEASUREMENTS

The photometric measurements were made with the PSF-fitting routine ALLSTAR (Stetson & Harris 1988). The source catalogues, PSFs, and aperture photometry that are used by ALLSTAR were obtained by running tasks in the DAOPHOT package (Stetson 1987). The PSFs for each sub-mosaic were constructed from 50 – 100 stars that were selected according to brightness, appearance, and an absence of bright neighbors. Faint stars in the vicinity of the PSF stars were removed in an iterative manner, being subtracted from the images using progressively improved versions of the PSF.

ALLSTAR iteratively rejects sources that have poor photometric measurements. Despite such culling, a fraction of the sources in the photometric catalogues produced by ALLSTAR have measurements that are suspect, and these should be identified and rejected. As in previous photometric studies of stars in nearby galaxies (e.g. Davidge 2010), sources were culled from the photometric catalogue using criteria based on the uncertainty in the magnitudes calculated by DAOPHOT, ϵ .

All objects with $\epsilon > 0.3$ mag were excised from the catalogues, as useful photometric information can not be obtained for these sources, the vast majority of which are at the faint limit of the data. In addition, objects that depart from the trend between ϵ and magnitude defined by point sources in each field were also removed. As demonstrated in Figure 2 of Davidge (2010), the objects rejected in this step tend to be non-stellar in appearance, with the majority being galaxies, stellar blends, or cosmetic defects. At intermediate and brighter magnitudes this filtering may reject up to a third of all sources.

3.1. Calibration

Photometric standard stars are observed during each MegaCam run, and the calibration information generated from these observations is inserted into the image headers as part of the ELIXER processing. The photometry used in this paper was calibrated using this

information. The u^* measurements were transformed into u' magnitudes.

Massey et al. (2006) investigated the UBVRI properties of the brightest stars in M33, and their catalogue can be used to check our calibration. The spatial coverage of the Massey et al. (2006) survey restricts these comparisons to the Central Field. The comparisons were restricted to only the brightest stars that fall outside of the main body of the disk to minimize the impact of crowding. The Massey et al. (2006) and MegaCam data were recorded during different epochs, and so variable stars will contribute to the scatter between the two sets of measurements.

u' and g' magnitudes for stars in the Massey et al. (2006) catalogue were calculated using the empirical transformation relations found by Smith et al. (2002). The CMD of the stars that were used to check the measurements is shown in the top panel of Figure 2. While the sample contains sources with intermediate and blue $u' - g'$ colors, the majority of sources have red $u' - g'$ colors. This is a consequence of restricting the comparison sample to stars outside of the crowded star-forming disk of M33.

The difference between the two sets of measurements, $\Delta u'$, in the sense CFHT – KPNO, is shown as a function of $u' - g'$ in the lower panel of Figure 2. The mean $\Delta u'$ is 0.04 ± 0.06 magnitudes, where the quoted uncertainty is the formal error of the mean. The Spearman correlation coefficient between $\Delta u'$ and $u' - g'$ is -0.34 , indicating that there is not a significant correlation between these quantities. The scatter about the calibrating relation between $u' - g'$ and $U - B$ in Figure 13 of Smith et al. (2002) is roughly ± 0.1 magnitudes. If the four outliers with large $|\Delta u'|$, which are probably variable stars, are not considered then the majority of $\Delta u'$ values fall within the ± 0.1 magnitude dispersion expected based on the scatter in the empirical relation between $u' - g'$ and $U - B$. We conclude that the good mean agreement between the CFHT and NOAO measurements indicates that the photometric calibration is reasonably sound.

3.2. Artificial Star Experiments and Data Characterization

The uncertainty computed for magnitudes measured by ALLSTAR is based on the quality of the PSF fit, but does not account for systematic errors that might result from – say – crowding; thus, it gives only a lower limit to the actual uncertainties in the photometric measurements. Supplementary information about the photometric uncertainties in ensembles of stars, rather than individual sources, can be obtained from artificial star experiments. These experiments have the merit of also providing information about sample completeness.

Main sequence stars are the primary targets of this investigation, and so the artificial

stars were assigned magnitudes and colors that fall along the observed main sequence ridge-line. As with actual stars on the sky, artificial stars were only considered to be recovered if they were detected in both filters. The photometry files produced in the artificial star experiments were also culled using the ϵ -based criteria described earlier.

The incidence of blending and the random errors in the photometry both increase rapidly with magnitude when the completeness fraction drops below 50%, and so the magnitude at which 50% completeness occurs provides a simple metric for gauging the faint end of the useable data range. The distribution of stars in the M33 disk means that the 50% completeness magnitude changes with location in the Central Field, and the artificial star experiments indicate that 50% completeness occurs near $u' = 24$ at $R_{GC} = 5$ kpc (18 arcmin), and $u' = 25.3$ at $R_{GC} = 9$ kpc (32 arcmin). For comparison, 50% completeness occurs near $u' = 25.6$ throughout the fields that were observed in 2009B.

The photometry was further characterized by comparing measurements made in overlapping sections of the fields. Such comparisons have the potential of revealing sources of error that are not addressed by the artificial star experiments. The difference in u' between sources common to both the NE and NW fields was found to have a roughly constant dispersion when $u' < 24$, amounting to $\sigma = \pm 0.03$ magnitudes. This is larger than predicted by the artificial star experiments, which predict a dispersion of ± 0.02 magnitudes at $u' = 22$.

Artificial star experiments require an input PSF, and for ground-based observations the PSF typically is constructed from the data. One consequence is that the uncertainties deduced from artificial star experiments do not account for PSF-matching errors, which will be present at some level in all datasets, as it is not possible to characterize the PSF in a perfect way. The NE and NW fields overlap at the edges of the MegaCam science fields where the PSF can vary over small spatial scales, and the constant dispersion in the difference between the photometric measurements in these fields over a range of magnitudes is consistent with the behaviour expected from PSF-matching errors.

PSF-matching errors due to spatial changes in the PSF can be quantified by computing aperture corrections, which are the differences between magnitudes measured using large apertures and those determined from PSF-fitting, at various points across a field. The aperture correction will vary across the field if there are changes in the PSF that have not been tracked. We have computed aperture corrections for bright, isolated sources in the section of the NE field that overlaps with the NW field. The aperture correction varies systematically with location across the field, in the sense of increasing in size towards the edge of the MegaCam field. The amplitude of the variation of the aperture correction is 0.06 magnitudes, which is in excellent agreement with the residual dispersion discussed above. We thus conclude that PSF-matching errors introduce uncertainties of a few hundredths of

a magnitude to these data.

4. AN OVERVIEW OF THE STELLAR CONTENT

4.1. Star-Forming Complexes

The disk of M33 contains a number of young stellar complexes, and the photometry of stars in such systems provides an empirical means of assessing the impact of crowding on the photometry in general. To this end, four associations/star-forming complexes – IC 133, A 31, A 116, and A 127 – were selected for study. The last three objects are from the catalogue of Humphreys & Sandage (1980). It should be emphasized that these are not star clusters in the traditional sense, but giant star-forming complexes of the type discussed by Efremov (1995). The sizes of these complexes may reflect the spatial scales for star formation defined by turbulence (Elmegreen et al. 2003).

These four particular complexes were selected because they are in isolated environments, thereby making their boundaries relatively easy to identify when compared with similar complexes in denser portions of the disk. The geometric center and radius for each complex were estimated by eye, and the CMDs of objects within the extraction regions are shown in Figure 3. These complexes span a range of source densities. Aperture photometry indicates that IC 113, A 31 and A 116 have comparable surface brightnesses, whereas A 127 is roughly 1 mag arcsec² brighter in u' and g' .

Even though these complexes are in isolated portions of M33, there is non-negligible contamination from disk stars. To allow the extent of this contamination to be assessed, the CMDs of sources in an annulus surrounding each complex, that subtends the same total area on the sky as the cluster that it abuts, were also constructed, and the results are shown in Figure 3. The number densities of sources near the faint ends of the background CMDs are higher than in the CMDs of the adjacent clusters, demonstrating the diminished impact of crowding in the (comparatively) low density circumcluster environments.

The main sequence is the dominant feature in the cluster CMDs. Because young stellar regions do not have hard boundaries, some fraction of the stars in the background regions are almost certainly cluster members; still, the brightest main sequence stars occur in the young complexes, rather than the background fields. Sources to the right of the main sequence are BSGs.

The CMDs of the young stellar complexes are compared with isochrones from Girardi et al. (2004) in Figure 4. The models have $Z = 0.008$, which is close to the metallicity

measured for BSGs in M33 by U et al. (2009). There is reasonable agreement between the predicted and observed main sequence color of A 31 over a large range of u' magnitude. This suggests that the baseline reddening is appropriate for this complex, and that crowding does not appear to affect the photometric measurements.

In the case of A 116, the stars with $u' < 22$ are well matched by the 10 Myr isochrone, but at fainter magnitudes many sources fall redward of the predicted main sequence. Because A 116 is a star-forming region then it is possible that the red objects may be stars that have not yet collapsed onto the main sequence. Still, for these to be pre-main sequence stars then the evolutionary tracks of Cignoni et al. (2009) suggest that there must have been a significant star-forming episode in A 116 within only the past few Myr. For comparison, the main sequence turn-off of A 116 is well matched by the 10 Myr isochrone.

The agreement between the observations and models is not as good for the other two complexes, with the locus of blue stars falling $\sim 0.1 - 0.2$ magnitudes redward of the zero age main sequence (ZAMS) for a young population. This could indicate that A_V is $\sim 0.2 - 0.3$ magnitude higher for these complexes than the baseline value. The effect of adopting a higher line-of-sight extinction is demonstrated in Figure 4, where the dashed line shows the 10 Myr isochrone with $A_V = 0.2$ mag additional extinction.

While the agreement with the observed color of the main sequence is improved somewhat with a higher extinction, the agreement at fainter magnitudes remains poor, in the sense that the majority of stars still fall to the right of the predicted ZAMS. A comparatively red main sequence near the faint end of IC 133 would occur if this structure contains stars that span a range of ages. Indeed, the main sequence in the CMD of this complex can be matched if it contains stars that formed during the past ~ 100 Myr. This timescale falls within the expected lifetime of large star-forming complexes (e.g. Davidge et al. 2011). However, this explanation does not hold for A 127, where the number of stars plunges near $u' = 22$.

In summary, even though these are relatively dense stellar aggregates, the photometry of stars with $u' < 22$ tends to be well matched by model isochrones. The one exception is A 127, which has the highest surface brightness of the four complexes studied. However, even in this complex the isochrones pass through the main sequence at $u' \sim 20$. These comparisons indicate that the photometry of main sequence stars with ages ≤ 10 Myr should be reliable in relatively dense environments of M33, and in §6 this is validated by number counts of sources throughout the disk. Of course, in the lower density portions of the disk the faint limit of the data will be such that stars with ages that are well in excess of 10 Myr can be examined.

4.2. The M33 Disk

The $(u', u' - g')$ CMDs of stars in various radial intervals in the Central Field are shown in Figure 5. The distances given in each panel are measured from the center of M33 in the plane of the disk. A disk inclination of 54 degrees was assumed (Pierce & Tully 1992).

The influence of individual large star-forming complexes are suppressed when stars from large swaths of the M33 disk are combined. The main sequence forms a prominent plume with $u' - g'$ between 0.0 and 0.5 in the $R_{GC} < 10$ kpc CMDs, and the diffuse spray of objects to the immediate right of the main sequence is dominated by BSGs. Source confusion increases with stellar density, and this can clearly be seen in the comparatively shallow faint limit in the CMDs for $R_{GC} < 4$ kpc. At the bright end, crowding is mitigated to some extent by the blue wavelength coverage of the u^* filter, which avoids the peak in the spectral-energy distribution of the majority of disk stars. The brightest blue objects in Figure 5 have $u' \sim 17$ when $R_{GC} < 8$ kpc, and that this peak brightness does not change with radius when $R_{GC} < 8$ kpc suggests that the incidence of blending is not significant amongst the brightest sources.

The properties of the CMDs in Figure 5 might be expected to change with radius based on results presented in previous studies. Munoz-Mateos et al. (2007) and Verley et al. (2009) present evidence that the fractional contribution made by young stars to the overall stellar content increases with radius in M33, although this trend ultimately reverses in the outer galaxy (Williams et al. 2009). Bastian et al. (2007) and Park et al. (2009) find that the number of young stellar groups and clusters drops near $R_{GC} = 4$ kpc. In contrast, Thilker et al. (2005) find that the FUV–NUV color is constant across the disk, with a value that is consistent with a flux-weighted age in the range 200 – 300 Myr, suggesting that the young stellar mixture does not change with radius. In fact, there is no obvious change in the properties of the main sequence stars and BSGs in the $R_{GC} < 8$ kpc CMDs in Figure 5.

Thilker et al. (2005) find that UV emission from the M33 disk drops at a radius of 30 arcmin ($R_{GC} = 8.5$ kpc), signalling a rapid decrease in recent star-forming activity. Signatures of such a drop in star-forming activity should also be evident in the $(u', u' - g')$ CMDs. In fact, a marked change in the brightness of the MSTO between the 6 – 8 kpc and 8 – 10 kpc CMDs is evident in Figure 5.

The mean color of main sequence stars in a given magnitude interval changes with radius. This is demonstrated in Figure 6, where the histogram distributions of $u' - g'$ colors for sources with u' between 20.5 and 21.5 in four annuli are compared. The prominent bump in the color distributions is due to main sequence stars, and the peak of this feature is displaced to progressively redder values with decreasing distance from the center of the galaxy. A least squares fit to the peaks of the color distributions indicates that $\Delta(u' - g')/\Delta(R_{GC}) =$

$-0.021 \pm 0.004 \text{ kpc}^{-1}$. The recent SFH of M33 does not change with radius in this part of the galaxy (§5), and so the change in main sequence color is not due to a systematic gradient in the SFH. Rather, the radial trend in mean color could be attributed to systematic changes in the amount of extinction. Adopting the reddening law in Table 6 of Schlegel et al. (1998) then gradients amounting to $\Delta E(B - V)/\Delta R_{GC} = 0.015 \pm 0.003 \text{ kpc}^{-1}$ and $\Delta A_V/\Delta R_{GC} = -0.05 \pm 0.01 \text{ kpc}^{-1}$ could explain the trends in peak main sequence color. Davidge (2007) also found evidence for higher levels of extinction among the youngest stars in the central few kpc of the Sc galaxy NGC 2403.

The widths of the color distributions do not change with radius when $R_{GC} < 6 \text{ kpc}$. The artificial star experiments predict a dispersion in $u' - g'$ of $\pm 0.04 \text{ mag}$ in the 4 – 6 kpc annulus, whereas the observed dispersion is $\sigma_{u'-g'} = \pm 0.135 \text{ mag}$. The width of the main sequence in these observations is thus not dominated by observational errors. A number of factors, such as evolution away from the ZAMS, differential reddening, binarity, and photometric variability will contribute to a main sequence that is wider than expected from observational uncertainties alone. An upper limit to the amount of differential reddening can be obtained by assuming that it is the dominant source of dispersion in $u' - g'$. After subtracting in quadrature the contribution made by observational errors, then we find that $\Delta E(B - V) \leq \pm 0.10$ and $\Delta A_V \leq \pm 0.3$ throughout the inner disk. For comparison, the scatter in reddening found by U et al. (2009) from AB supergiants is $\pm 0.04 \text{ mag}$ in E(B–V).

The CMDs are compared with $Z = 0.008$ isochrones from Girardi et al. (2004) in Figure 7. The isochrones track the locus of main sequence stars, as expected if the baseline reddening model applies to the majority of young stars throughout the M33 disk. Comparisons with the isochrones further indicate that the youngest stars in the 4 – 6 kpc interval have ages $\leq 10 \text{ Myr}$. However, at larger radii the ages of the youngest stars increases with galactocentric distance, such that in the 12 - 14 kpc interval the youngest stars have ages $\sim 100 \text{ Myr}$.

Star counts provide insights into the recent SFR. We consider the statistics of stars with ages $\leq 10 \text{ Myr}$ – which have masses $< 20 M_\odot$ – as these objects are present throughout the central 8 kpc of M33 (§6) and are less prone to crowding-related issues than fainter objects. With a global SFR of $0.7 M_\odot \text{ year}^{-1}$ (Blitz & Rosolowsky 2006), then $7 \times 10^6 M_\odot$ of stars will have formed in the past 10 Myr throughout M33. Adopting the Kroupa (2001) initial mass function (IMF) from 0.08 to $100 M_\odot$, then $8 \times 10^5 M_\odot$ of stars with masses in excess of $20 M_\odot$ will have formed. This translates into $\sim 10^4$ main sequence stars, and such objects will have $u' \leq 19.5$. For comparison, $\sim 3 \times 10^3$ objects with $u' \leq 19.5$ are seen throughout M33. Some of these bright objects are undoubtedly binaries or unresolved compact star clusters, and so the actual number of massive main sequence stars will be less than this.

There is roughly a factor of ~ 3 difference between the observed number of very bright stars and the number expected if the $\text{SFR} = 0.7 \text{ M}_{\odot} \text{ year}^{-1}$. Possible explanations for this discrepancy are that (1) the SFR has been lower than $0.7 \text{ M}_{\odot} \text{ year}^{-1}$ during the past 10 Myr, (2) many very young stars are missing, either because they are in unresolved blends or are heavily obscured, and hence are not detected, and/or (3) that the IMF in M33 may be skewed to the production of fewer massive stars than predicted by Kroupa (2001). We consider the first two of these to be more likely than the third, given that model LFs constructed with a Kroupa (2001) IMF match the slope of the observed LF of bright main sequence stars throughout M33 (§5). In §7 we argue that a SFR of $0.7 \text{ M}_{\odot} \text{ year}^{-1}$ is probably not sustainable in M33 for a prolonged period of time given the mass of the ISM.

4.3. The Outer Disk

The $(u', u' - g')$ CMDs of sources in the NE, NW, SE, and SW fields are shown in Figure 8. The source densities in these fields are lower than in the Center Field, and so the CMDs in Figure 8 extend to fainter magnitudes than is typical of the Center Field. The majority of sources with $u' - g' \geq 1$ and $u' > 24$ are background galaxies, although core Helium burning stars will also occupy this part of the CMD if an intermediate age population is present. Blue HB stars belonging to an old metal-poor component are too faint to be detected with these data.

There is a well-populated main sequence in the CMDs of the NE and NW fields, and many of the brightest main sequence stars belong to the two star-forming complexes in the northern spiral arm of M33 that were studied by Davidge et al. (2011). Bright main sequence stars are also seen in the CMD of the SW field, although there are fewer stars than in the NE and NW fields. The CMDs of the portions of the NE and SW fields that have the highest stellar densities are compared with $Z = 0.008$ isochrones from Girardi et al. (2004) in Figure 9. The areas from which sources were extracted to construct the CMDs in Figure 9 are indicated in Figure 17.

Whereas the brightest main sequence stars near the northern edge of the disk follow the 10 Myr isochrone, the majority of stars in the southern part of the disk have ages ≥ 10 Myr. The red envelope of the main sequence in both CMDs tracks the redward extent of main sequence evolution predicted by the isochrones. This is consistent with the majority of blue sources with $u' \geq 24$ in these areas being intermediate age stars, rather than background objects.

A rich population of objects with $u' - g' \sim 0.4$ and $u' > 23.5$ are seen in the CMDs of

all four fields. The photometric properties of these objects are consistent with them being main sequence stars with ages ≥ 100 Myr. While in reality a substantial fraction are either blue galactic nuclei or star-forming regions in background galaxies, it is demonstrated in §6 that some of these faint blue objects define structures in the outer regions of the M33 disk, and so are probably stars that belong to M33.

5. THE LFs OF MAIN SEQUENCE STARS AND THE STAR-FORMING HISTORY

5.1. Model LFs

The faint limit of these data is sufficient to allow the SFH during the past few hundred Myr to be probed using the u' LF of main sequence stars. The structural properties of main sequence stars are subject to fewer uncertainties than those of more evolved objects, making model LFs of main sequence stars potentially more reliable probes of SFH than the LFs of stars in advanced stages of evolution. The affect of uncertainties in the advanced stages of stellar evolution on SFHs has been investigated by Melbourne et al. (2010), who compare SFHs of the dwarf galaxy KKH 98 deduced from AGB and main sequence stars. These two stellar types yield SFHs that differ significantly during intermediate epochs, and this is attributed to uncertainties in the physics of AGB evolution. Still, our knowledge of main sequence evolution is not ironclad, and uncertainties in the mechanics of mass loss, coupled with an incomplete knowledge of convection – the dominant source of energy transport in the central regions of massive stars – are some of the deficiencies that affect models of massive stars as they evolve off the ZAMS, but are still burning Hydrogen in their core.

Binarity is not an issue when modelling more evolved stages of evolution at visible wavelengths, as the more massive star in a pair evolves from the main sequence first. The light of the primary then swamps that of its less massive (and hence less evolved) companion(s). Binarity is a concern when modelling the characteristics of main sequence stars at visible wavelengths as brightness differences between the primary stars and any companions are much smaller than if one star is highly evolved. However, as long as the binary fraction and mass ratio characteristics do not change with the mass of the primary then the overall *shape* of main sequence model LFs will not be affected greatly by binarity. In recognition of this issue, comparisons with model LFs are restricted to LF shape, rather than the absolute predictions of star numbers predicted by the models.

Model LFs were constructed from isochrones in the Girardi et al. (2004) compilation using routines in STARFISH (Harris & Zaritsky 2001). IMF with mass function exponents

$\alpha = -2.7$ (Kroupa et al. 1993) and $\alpha = -2.3$ (Salpeter 1955) for massive stars were considered. The models assume $Z = 0.008$. There is a radial metallicity gradient in the inner disk of M33 (e.g. U et al. 2009), and models with lower metallicities than this may be more appropriate for comparisons with outer disk LFs. However, the structural properties of ZAMS stars in the range of stellar masses considered here ($> 3 M_{\odot}$) is not sensitive to metallicity.

The model LFs are used as interpretive tools, and no attempt is made to model particular features in the observations. To this end, models were generated for two SFHs that provide useful diagnostic information. One set of models assumes simple stellar populations (SSPs), in which the component stars are coeval and have a single metallicity. While SSP models are strictly appropriate only for star clusters, these models may approximate the bright end LFs of systems that have undergone a single large star-forming event during recent epochs.

The second set of models assumes a SFR that is constant with time. Such a SFH might be expected to dominate in undisturbed disks if stochastic effects are suppressed by averaging over large areas and long time intervals. The metallicities of stars that form during constant SFR conditions will grow steadily with time, as previous stellar generations process and recycle interstellar material. While our models do not account for such enrichment, it is anticipated that this will not significantly affect the results. Indeed, the age-metallicity relation in the M33 disk during the time interval that we explore – the past few hundred Myr – has been flat (Magrini et al. 2009). Even if an age-metallicity relation that is appropriate for the Solar neighborhood were to hold, it would result in only marginal enrichment over the ~ 200 Myr time interval that is sampled by the stars examined here.

5.2. Comparisons with Model LFs

The LFs of objects in the M33 disk with $u' - g'$ between -0.5 and 0.5 , which is the color interval that is dominated by massive main sequence stars, are shown in Figure 10. The faint limit in the 0 - 2 and 2 - 4 kpc LFs is markedly brighter than at larger radii owing to the higher stellar densities in these intervals. Source counts from the outer regions of the NE field, where the density of bright stars that belong to M33 should be negligible, have been subtracted to account statistically for contamination from foreground stars and background galaxies. This correction has only a modest impact on the $R_{GC} \leq 10$ kpc LFs.

The shape of the LFs in Figure 10 changes with radius. Williams et al. (2009) conclude that the stellar content of M33 changes significantly near 8 kpc, and Thilker et al. (2005) find

a drop in the level of UV emission and a change in the FUV–NUV color at this point. It is thus worth noting that the character of the LFs in Figure 10 also changes near $R_{GC} = 8$ kpc. The LFs of sources with $R_{GC} \leq 8$ kpc follow a single power-law with a common exponent, whereas at larger radii the LFs at the bright end flatten. The number of sources with $u' \leq 20$ also drops near $R_{GC} \sim 10$ kpc, although this may be due to small number statistics.

Three LFs from Figure 10 are compared with the SSP and constant SFR model LFs in Figures 11 and 12. The models have been scaled to match the number densities of objects with $M_{u'}$ between -2 and -4 . It is apparent from Figure 11 that the SSP models are much flatter than the observed LFs, indicating that the young stars in the M33 disk formed over a range of epochs, and not in a single large-scale event.

In contrast to the SSP models, the constant SFR models in Figure 12 are an excellent match to the $6 - 8$ kpc and $8 - 10$ kpc LFs in the interval $M_{u'} \leq -2$. The agreement is noteworthy given that no effort was made to tune the models to match the observations. The agreement with the $10 - 12$ kpc LF is much poorer, in the sense that the slope of the observed LF is not reproduced at the faint end, and the fractional contribution made by older stars is higher than expected from a constant SFR in this radial interval. The absence of stars with $M_{u'} < -5$ in this radial interval may be due to small number statistics, as only a few are expected in this brightness range under the assumption of a constant SFR.

The ISM of M33 is not distributed symmetrically throughout the galaxy (e.g. Verley et al. 2010), and so region-to-region variations in the SFH of the M33 disk might be expected. To assess the amplitude of possible large-scale azimuthal SFH variations throughout the M33 disk, the LFs of sources in two of the annuli examined in Figures 11 and 12 were constructed using 90 degree azimuthal gathers, as opposed to the 360 degree gather used to construct the LFs in Figure 10. The four resulting LFs in each radial interval are compared in Figure 13.

There are only minor quadrant-to-quadrant variations at the faint end of the LFs in Figure 13. This is perhaps not unexpected given that progressively fainter magnitude intervals contain main sequence stars that formed over wider ranges of epochs than at the bright end, with the result that variations in SFH average out. However, the situation is very different near the bright end. While small number statistics are a factor amongst the brightest stars, in the interval between $M_{u'} = -3.5$ and -1.5 the quadrant-to-quadrant differences are larger than predicted by random errors alone. A systematic difference between the LFs of the northern and southern halves of the galaxy is evident in this magnitude interval, in the sense that the source density in the south is ~ 0.4 dex higher than in the north. This suggests that the SFR during the past ~ 100 Myr in the southernmost part of the disk has been $\sim 2\times$ that in the northernmost part. This is consistent with the southern part of the

disk having a higher HI concentration than the northern part (e.g. Verley et al. 2010).

6. THE PROJECTED SPATIAL DISTRIBUTION OF MAIN SEQUENCE STARS

6.1. The Large-Scale Distribution of Disk Stars

The distribution of sources in the Central Field, selected from the $(u', u' - g')$ CMD using the photometric criteria defined in Figure 1 of Davidge et al. 2011 for characteristic ages of 10 and 100 Myr, are shown in Figure 14. The on-sky source distribution is shown in the top row, while the de-projected distribution, approximating the appearance of M33 as if viewed face-on, is shown in the bottom row. Depth effects have only a minor impact on the de-projected distribution given the moderate inclination of M33 to the observer.

The star counts drop markedly at 25 – 30 arcmin radius, or 7 – 8 kpc, and this is the point at which UV emission also drops (Thilker et al. 2005). It is also evident from Figure 14 that stars in the 10 and 100 Myr samples have very different distributions, in that much more clustering and spiral structure is evident in the 10 Myr sample than in the 100 Myr sample. The lack of objects in the 100 Myr sample throughout the central regions of M33 is due to crowding.

The uniform distribution of sources in the 100 Myr sample is largely a consequence of the random motions imparted to objects through interactions with giant molecular clouds, which in turn causes them to diffuse from their places of birth with time. Other processes, such as the churning of stellar orbits by spiral density waves (Sellwood & Binney 2002), further blur the stellar distribution, although these are expected to act over time spans of a few disk rotations, and so should not affect the locations of the stars that are considered in the present study, the oldest of which have an age of only \sim one disk rotation.

6.2. The Radial Distributions of Young and Old Stars

Bakos et al. (2008) find that the luminosity-weighted ages of Type II disks (i.e. those that – like M33 – have a downward-breaking light profile at large radii) at visible wavelengths is a minimum at the break radius. Based on the color profiles of these systems, they argue that the break in the light profile is a consequence of the luminosity-weighted age profile of the disk, rather than a discontinuity in the disk mass distribution. There is a possible physical driver for this behaviour, as cosmologically-based models of late-type spiral galaxies find

that the ratio of gas to stellar mass peaks at the break radius, fostering a higher proportion of young stars at this point than elsewhere in the disk (Martinez-Serrano et al. 2009).

How do the radial distributions of young and old stars compare in M33? Verley et al. (2009) investigated the light profile of M33 at wavelengths ranging from $3.6\mu\text{m}$ to $160\mu\text{m}$. While the light at mid and far-infrared wavelengths is thermal in origin, and hence traces interstellar and circumstellar material, at $3.6\mu\text{m}$ the light originates predominantly from the photospheres of cool stars, and so observations at this wavelength can be used as a proxy for overall stellar mass. With the exception of an upturn in the innermost regions of the galaxy, the $3.6\mu\text{m}$ light profile of M33 shown in Figure 2 of Verley et al. (2009) follows a single power law between 1 and 9 kpc; thus, there is no evidence for a break in the stellar mass distribution near 8 kpc.

The number density of objects in the 10 Myr sample is compared with the $3.6\mu\text{m}$ integrated light profile from Figure 2 of Verley et al. (2009) in Figure 15. The $3.6\mu\text{m}$ relation has been adjusted to account for the slightly larger distance to M33 adopted for the present study. The zeropoint of the $3.6\mu\text{m}$ profile has also been adjusted so that the curve passes through the midpoint of the 10 Myr star counts.

The 10 Myr star counts define a trend that is flatter than the $3.6\mu\text{m}$ integrated light profile at $R_{GC} < 8$ kpc, indicating that the contribution made by young stars to total stellar mass grows with increasing radius in the central 8 kpc. In addition, that the 10 Myr star counts define a more-or-less linear relation for $R_{GC} \geq 1.5$ kpc suggests that incompleteness is not an issue for these very bright stars throughout much of the M33 disk. The number density of young stars drops near $R_{GC} \sim 8$ kpc, whereas the character of the $3.6\mu\text{m}$ profile does not change at this point. The HI distribution of M33 has been mapped over a large area, and there is a localized maximum in HI emission near 7 kpc (e.g. Figure 3 of Corbelli 2003), which is close to the radius at which young stars make the largest contribution to the stellar mass density. The contribution that the youngest stars make to the total stellar mass drops near $R_{GC} = 8$ kpc; the radial distributions of young and old stars in the M33 disk are thus consistent with that found in other systems by Bakos et al. (2008).

In §5 it was shown that the recent SFH of the M33 disk changes near 8 kpc, in the sense that at smaller radii the SFR during the past few hundred Myr has been continuous, while outside the break radius there has been reduced star-forming activity over the past few tens of Myr when compared with the past few hundred Myr. The drop in the number density of very young stars near $R_{GC} = 8$ kpc, coupled with the continuous trend defined by $3.6\mu\text{m}$ light, suggests that the SFR at large radii was not elevated during intermediate epochs. Rather, it is more likely that the SFR in the outer disk dropped during the past ~ 100 Myr.

The decrease in the numbers of young stars at $R_{GC} > 8$ kpc is probably due in part to the asymmetric distribution of gas in the outer regions of M33. To the extent that HI traces molecular material, the HI distribution mapped by Putman et al. (2009) suggests that large portions of the circumdisk environment are devoid of star-forming material. Another factor is that the density of star-forming material throughout the M33 disk is sub-critical (Martin & Kennicutt 2001), and the probability of breaching the threshold for star formation is low in the outer regions of M33. Finally, the basic properties of star-forming material may change with radius in M33. Evidence for this comes from the physical sizes of molecular clouds in M33, which appear to decrease in size towards larger radii (e.g. Gratier 2010). Such a trend will affect the sizes of star-forming regions at large radii, which in turn may affect the chances of forming massive stars.

6.3. The Spatial Distribution of Young Stars on Sub-Kiloparsec Scales

We use the star-star separation function (S3F) to investigate stellar grouping throughout the M33 disk. The S3F, which was defined by Davidge et al. (2011), is the histogram distribution of separations between all possible stellar pairings. Davidge et al. (2011) used the S3F to investigate the distribution of main sequence stars in the peripheral regions of M33, and significant projected spatial coherence was detected among the youngest stars over separations ≤ 0.7 kpc. The degree of coherence in the sample of objects studied by Davidge et al. (2011) was found to decrease with increasing stellar age, and it was concluded that star-forming complexes in this environment dissipate over time spans of a few tens of Myr.

The S3Fs of M33 disk stars in two radial intervals are compared in Figure 16. The current investigation is restricted to stars in the 10 and 40 Myr samples because of the substantial level of incompleteness in the 100 Myr sample at small radii. In addition, as we are interested in stellar grouping on kpc and smaller spatial scales, the comparisons are limited to separations ≤ 2 kpc, or roughly one disk scale length. The signal in each interval has been normalized to the number of objects with separations between 0.5 and 1.5 kpc (110 to 330 arcsec).

The shape of the S3Fs in Figure 16 differ from those examined by Davidge et al. (2011), in that prominent peaks at moderate separations are absent. Davidge et al. (2011) studied a comparatively small area on the sky in the outer disk of the galaxy that included two large star-forming complexes, so that there was a bias towards small separations. In contrast, the S3Fs in Figure 16 are constructed from stars that cover large swaths of the disk, so that the influence of single star-forming complexes on the S3F are suppressed.

The S3Fs of the 40 Myr sample are steeper than those in the 10 Myr sample at separations between 0 and 200 arcsec (i.e. between 0 and 1 kpc). There is thus greater spatial coherence among stars in the 10 Myr sample with separations < 60 arcsec (< 250 parsecs) than in the 40 Myr sample. The reduced signal at small separations in the 40 Myr sample indicates that stars in the disk of M33 become less tightly grouped over timescales of only a few tens of Myr, due to the diffusion of stars from their places of birth.

6.4. Diffuse Structures at the Disk Boundary

Structures of a tidal origin lack a dark matter cocoon, and so their morphology can evolve over timescales that are short when compared with classical galaxies. Indeed, while the disruption timescale for structures in the outer regions of galaxies is comparatively long (e.g. Johnston et al. 1996), the prognosis for the long term survival of tidal structures is poor, with the vast majority expected to dissipate over time spans of only a few hundred Myr (Bournaud & Duc 2006). Still, some structures may survive over Gyr or longer timescales if the interaction geometry is favorable; for example, long-lived tidal features may form if the orbit of the perturber is more-or-less coplanar with the disk of the host galaxy (Bournaud & Duc 2006).

The stellar content of a tidal feature provides a direct means of probing its history. A critical piece of information that can be gleaned from the stellar content is the age of the structure, which in turn indicates when the interaction occurred. A tidal arm that is pulled from a star-forming disk in an interaction that occurred during cosmologically-recent epochs should contain stars that span a wide range of ages, reflecting the extended SFH of the original disk. If the donor was actively forming stars before the interaction then some of the youngest stars in a tidal stream will have formed only shortly before the interaction. However, these may not be the youngest stars in the structure, as stars may form for some period of time after an interaction if local density enhancements persist in the gaseous component of the debris field.

Evidence for low-level on-going star-forming activity is seen in extragalactic debris fields. The nearest example is the region between M81 and M82 (e.g. de Mello et al. 2008), even though the interaction occurred a few hundred Myr in the past (Yun et al. 1994). In addition to star-forming structures, the M81–M82 debris field also contains a number of low density young stellar groupings that appear to have formed during the past few tens of Myr, but are not forming stars at present (e.g. Davidge 2008; Mouchine & Ibata 2009). These objects suggest that there was likely larger scale star-forming activity in the debris field in the not too distant past.

Whether or not stars form depends on the conditions in the debris field, including the density of star-forming material. There is evidence of tidal material in the circumdisk environment of M33. The ridgeline of the HI distribution mapped by Putman et al. (2009) defines an S-shaped morphology, with arms that extend to the north west and to the south east of the disk. However, whereas the HI density throughout much of the M81–M82 debris field is $10^{21} - 10^{22} \text{ cm}^{-2}$ (Yun et al. 1994), comparable densities are found only in the main disk of M33 (Putman et al. 2009). Indeed, the HI density in the arms that emerge to the north west and south east of the M33 disk is an order of magnitude lower than is seen in much of the M81–M82 debris field.

A stellar structure that may coincide with one arm of the HI emission is discussed by McConnachie et al. (2009; 2010). If the stars in this structure are tidal in origin then they presumably were pulled from the disk during the most recent interaction with M31. In fact, simulations of interactions between M31 and M33 discussed by McConnachie et al. (2009) produce structures that are similar to those detected near M33, while also predicting significant warping of the M33 disk. However, McConnachie et al. (2010) measure a mean metallicity $[\text{Fe}/\text{H}] \sim -1.6$ for RGB stars in this feature, and such a low metallicity argues ostensibly against a disk origin. Still, if a large population of RGB stars with ages less than a few Gyr are present – as would be expected if these stars originated in a star-forming disk environment – then the metallicity estimated from color information will be skewed to low values if the calibration assumes that the RGB stars are all ‘old’.

The distribution of sources with magnitudes and colors that fall within the 100 Myr boundaries defined in Figure 1 of Davidge et al. (2011) is shown in Figure 17. The source distribution is more-or-less uniform over large fractions of the northern and southern fields. A visual examination of individual sources in the 100 Myr sample indicate that many of the objects in these fields are either background galaxies or individual star-forming regions in the spiral arms of moderately distant spiral galaxies that evaded the culling described in §3.

The substantial contamination by background galaxies notwithstanding, stellar groupings that are associated with the northern and southern end of the M33 disk are evident. Of particular note is the distinct spur of objects that extends to the north of the spiral arm, which will be referred to as the Northern Spur. Similar features do not emanate from the southern portion of the M33 disk.

The CMDs of sources in the Northern Spur and the Northern Disk, where the latter region is identified in Figure 17, are compared in Figure 18. These structures have very different stellar contents, in that the Northern Spur lacks the very bright main sequence stars that populate the Northern Disk. The majority of blue sources in the Northern Spur have $u' > 23.5$, which corresponds to ages in excess of 100 Myr. The Northern Spur thus

does not host obvious on-going star formation. Still, the Northern Spur may not be devoid of star-forming material, as the Putman et al. (2009) HI map shows a nose in the HI emission map that coincides with this structure.

The outer regions of M33 thus may contain at least one stellar grouping – the Northern Spur – that coincides with a region of HI emission. Given the evidence for an interaction with M31 as recently as 1 Gyr in the past, then the Northern Spur might be the remnant of a structure that formed due to the interaction, and in §6.5 it is demonstrated that it is part of a much more diffusely distributed structure. Structures of this nature may dissipate over a few disk rotation timescales, or \sim Gyr.

6.5. Mapping Very Diffuse Structures

There are indications that extremely diffuse intermediate age structures lurk in the peripheral regions of M33. While contamination from background galaxies complicates efforts to identify such objects, diffuse stellar aggregates can still be detected using source counts that are averaged over large angular scales. Such structures are hard to detect in unsmoothed star counts.

The distribution of 100 Myr objects in all five fields is shown in Figure 19. These images show star counts in 500×500 MegaCam pixel gathers. This bin size corresponds approximately to 0.5×0.5 kpc, and so is conducive to the detection of objects with spatial scales of a kpc or higher. A low pass filter was applied to the raw number counts to suppress isolated concentrations of objects that occur on scales of a few hundred MegaCam pixels, as visual examination indicates that many of these tend to be star-forming knots in moderately distant background galaxies.

In addition to the main body of the M33 disk, four distinct structures are seen in Figure 19. One of these is a low density extension of the Northern Spur. The connection between this structure and the disk is examined further in Figure 20, which shows the distribution of sources in the NE and NW fields, again with 500×500 MegaCam binning. The plume that contains the Northern Spur can be traced over ~ 25 arcmin, or ~ 7 kpc.

Three conspicuous extended structures are labelled DO (‘Diffuse Object’) 1 – 3 in Figure 19. The surface density of DO 2 is high enough that it can be seen in the upper right hand corner of the 100 Myr distributions in Figure 14. The compact nature of DO 3 is suggestive of a background cluster of galaxies. However, such a rich galaxy cluster is not obvious in the MegaCam data, and it is significant that – like DO 2 – DO 3 is located close to structure in the HI isophotes shown in Figure 1 of Putman et al. (2009), which is

reproduced in Figure 19.

DO 1 is located near the middle of the NE+NW fields, and is due north of M33. It is evident from Figure 20 that DO 1 may be connected to the main body of the M33 disk and the Northern Spur by a diffuse stellar bridge, as the sources counts to the south and south east of DO 1 are higher than to the north or west. A tongue of objects also extends south of DO 1, pointing directly to the M33 disk. DO 1 is ~ 0.5 degree East of the ridgeline of the HI arm mapped by Putman et al. (2009), and is at the eastern edge of the area labelled ‘S2’ in Figure 8 of McConnachie et al. (2010). That stars with ages of a few hundred Myr are seen near the McConnachie et al. (2010) structure raises the possibility that it may contain stars that span a range of ages.

The presence of blue stars with ages ~ 100 Myr suggests that star formation occurred in DO 1 (as well as DO 2 and 3) in the not too distant past. DO 1 is spread over ~ 400 arcmin² (~ 30 kpc²), and thus is comparable in extent to areas of UV emission in the outer regions of M83 (Thilker et al. 2005b). XUV disks occur in only a fraction of nearby galaxies (e.g. Zaritsky & Christlein 2007), and the so-called Type I XUV disks, in which the UV emission is clumpy rather than smoothly distributed, are likely the result of spiral structure propagating through the outer regions of disks (Bush et al. 2010).

While M33 does not have an XUV disk at the present day (Thilker et al. 2005a), there are hints that M33 may have experienced vigorous star-forming activity at large radii within the past few hundred Myr. There is a relative excess of stars that formed ≥ 100 Myr in the past at distances in excess of 8 kpc from the galaxy center (§5), and azimuthal mixing of tidal streams may contribute to producing such a diffuse stellar component (e.g. Oh et al. 2008). This being said, at least some of the older stars in the peripheral parts of the M33 disk may not have formed *in situ*, but may have migrated there as a result of dynamical interactions. Kinematic heating by sources that are external to the disk but still part of the extended dark matter field of the galaxy might also affect the distribution of stars at large radii (e.g. de Jong et al. 2007).

If star formation in DO 1 occurred *in situ* then M33 may have had an XUV disk ~ 100 Myr in the past. Alternatively, DO 1 may be the remnants of a stellar tidal stream, and this is supported by the close proximity to the structure identified by McConnachie et al. (2010). Deep imaging studies provide a means of distinguishing between these possibilities. Both the XUV and tidal source models predict that DO 1 should contain main sequence stars that are fainter than those found here. However, the XUV and tidal stream models predict different main sequence LFs. Whereas XUV activity should produce main sequence stars with a LF that follows that of a SSP, if DO 1 contains disk stars that span a range of ages then the main sequence LF should depart significantly from that of a SSP.

7. DISCUSSION & SUMMARY

Local Group galaxies are fundamental calibrators for stellar content investigations of more distant systems, many of which are late-type spiral galaxies. As the nearest Sc galaxy, M33 is thus an obvious target for understanding the pedigrees of more distant galaxies. In this study, moderately deep wide-field images recorded with the CFHT MegaCam have been used to probe the recent star-forming history of the M33 disk and its immediate surroundings. Main sequence stars that formed within the past few hundred Myr are resolved throughout a significant fraction of the ~ 4.5 degrees² that we examine.

Our study yields three main results. First, the LF of main sequence stars indicates that – when averaged over large parts of the disk – the SFR within the central 8 kpc of M33 has not changed with time during the past few hundred Myr. This in turn suggests that the disk has not been disturbed for at least this period of time, given that tidal interactions will affect the SFR by – for example – re-distributing star-forming material.

Second, the LF of main sequence stars at distances in excess of 8 kpc from the galaxy center is not consistent with a constant SFR during recent epochs. In fact, the peripheral regions of M33 are not locations of star formation at the present day, and the projected density of very young main sequence stars shows a steep drop near $R_{GC} = 8$ kpc. This radial truncation in the young star-forming disk is a robust result, that is also seen in the distribution of UV light (Thilker et al. 2005).

Third, we have found that the outer regions of M33 harbor diffuse collections of blue objects with photometric properties that are consistent with those of main sequence stars with ages ~ 100 Myr. Some of these structures appear to emerge from the disk, while others may be isolated. These structures may be tidal in nature, and/or may be spatially extended areas where star formation occurred *in situ*. The latter interpretation opens the possibility that while star formation at the present day is restricted to within ~ 8 kpc of the galaxy center, during intermediate epochs it may have occurred over a much larger region. The appearance of M33 at this time would have been very different from today, especially in the UV.

7.1. Evidence for an Interaction in the SFH, and the Long-Term Impact on M33

A centrally concentrated upswing in star-forming activity is one consequence of a tidal encounter with another galaxy. Tidal torques remove angular momentum from gas in the disk, causing it to migrate inwards. Elevated levels of star formation in the inner regions

of the galaxy are then triggered as the gas density builds and cools. Pre-existing stars in the disk gain angular momentum via interactions with the infalling gas clouds, and move to larger radii, producing an excess of old and intermediate age stars in the outer disk (e.g. Younger et al. 2008). If there was a recent interaction with M31 then elevated levels of central star formation may have occurred in M33 – is there evidence of such activity in the resolved stellar content?

If the disk of M33 is recovering from an uptick in star-forming activity that occurred within the past few hundred Myr, which is the typical timescale for a starburst, then the SFR should decrease as one moves towards more recent epochs. Such a decrease in the SFR is expected as the gas supply is depleted by star formation and/or feedback. Surveys of M33 star clusters suggest that a large peak in star-forming activity may have occurred ~ 0.1 Gyr in the past (Chandar et al. 1999). However, the excellent match between the observed LFs and constant SFR models within 8 kpc of the galaxy center indicates that the global SFR has not changed during the past ~ 0.2 Gyr. In fact, given that interactions fuel elevated levels of star formation over roughly a disk rotation time (~ 0.3 Gyr), then the results presented in this paper suggest that an interaction with M31 could not have occurred during the past $\sim 0.2 + 0.3 = 0.5$ Gyr.

Studies that examine older stellar generations provide additional constraints as to when an interaction between M31 and M33 may have occurred. Williams et al. (2009) find that the SFR near the center of M33 peaked during the past 0.5 – 2.5 Gyr, at which time the SFR jumped by an order of magnitude above the level that prevailed 2.5 – 10 Gyr in the past. The time at which this jump in the SFR occurred falls within the constraints set by the present-day positions and motions of M31 and M33 (Putman et al. 2009). Williams et al. (2009) also find that (1) the SFR varied with radius, as expected if gas is displaced by an interaction, and (2) the relative amplitude of the increase in the SFR during this same time interval drops with increasing R_{GC} , also as expected in the context of inward radial gas flows.

The global SFR during the past few hundred Myr has been lower than the long-term average (Williams et al. 2009), and the sSFR of M33 is lower than in most other late-type galaxies (Munoz-Mateos et al. 2007). These results are consistent with the depletion of cool gas throughout M33, as might occur if there was sustained large-scale star formation during intermediate epochs. The substantial jump in the central SFR during intermediate epochs and the subsequent drop in the SFR since that time suggests that M33 may have experienced a modest starburst; however, any starburst activity was not so dramatic as to present-day restrict star-forming activity to the central few kpc, as is seen in M82, where a large fraction of the outer stellar disk has been denuded of gas.

The drop in the infall rate 3 Gyr in the past inferred from the chemical enrichment properties of the outer disk of M33 by Barker & Sarajedini (2008) may be understood in the context of the stripping of the circumgalactic M33 HI reservoir by M31. The drop in infall occurred at a time that is consistent with the interaction timescales estimated by Putman et al. (2009). The disruption of such a circumgalactic reservoir will affect the overall appearance of M33 in two ways.

First, the removal of gas from the outer halo of a galaxy may affect the size of the star-forming disk. Models of ram pressure stripping indicate that star-forming disks contract as the circumgalactic gas reservoir that fuels star-forming material is removed (e.g. Bekki 2009). Of course, the Local Group environment is such that M33 has not been subjected to significant ram pressure stripping. Still, if the M33 gas reservoir was disrupted tidally then the net impact on the star-forming disk may be similar to that produced by ram pressure stripping: the appearance of a compact star-forming disk for an extended period of time (presumably a significant fraction of the Hubble time) until an external gas reservoir is restored. The sharp outer disk boundary at 8 kpc in M33 may be a consequence of a truncated angular momentum content in the circumgalactic gas reservoir.

Second, the removal of an external reservoir that replenishes disk gas will change the SFR, and hence the appearance of the galaxy. If the SFR during the past few hundred Myr has been $0.7 \text{ M}_\odot \text{ year}^{-1}$ (Blitz & Rosolowsky 2006), then $0.7 \times 0.2 \times 10^9 = 1.4 \times 10^8 \text{ M}_\odot$ of stars have formed in the past 0.2 Gyr. Adopting a 5% star formation efficiency (Inoue et al. 2004), then this level of star formation requires $2.8 \times 10^9 \text{ M}_\odot$ of gas. This is substantially lower than the present-day HI mass of M33 (Putman et al. 2009). To be sure, gas is recycled throughout the disk; still, the point to be made is that M33 is not gas-rich and the SFR, which has been constant for the past few hundred Myr, will gradually drop as the disk gas supply is depleted. The drop in SFR during the past 10 Myr that is predicted by the star counts in §4.2 may signal the start of this process.

7.2. The Distribution of Stars and Gas in M33 as a Probe of Interaction Timing

The radial distributions of gas and stars provide clues into the evolution of disks. Gas and stars are expected to have different distributions in isolated disks. This is due in part to the disk assembly process, as the angular momentum distribution of accreted gas will differ from that of stars that are already present. However, even in the absence of gas accretion, the distinct dynamical behaviours of stars and gas results in different radial distributions. Because of their small cross-sections when compared with typical stellar separations, stars

form collisionless systems, while the relatively large cross-sections of gas clouds make them collisional systems. Stars may also evolve into extraplanar systems that are distinct from the gas distribution, even in isolated galaxies. Indeed, some fraction of disk stars at small radii may evolve into a thick disk, as a natural consequence of inside-out disk formation (e.g. Schonrich & Binney 2009).

The distributions of gas and stars in disks have been modelled, and the results can be compared with the observed distributions in M33. Here, we consider the cosmologically-based galaxy simulations examined by Martinez-Serrano et al. (2009). A break in the model light profile typically occurs at ~ 3 disk scale lengths. The gas distribution in these models is roughly flat within the break radius, and gradually decreases beyond this point. Star formation continues past the break radius, occurring out to 4.3 scale lengths, at which point it ceases due to the low density of star-forming material. The ratio of gas mass to stellar mass peaks at the break radius, making this the point in the disk with the lowest photometrically-weighted age.

The HI density profile throughout much of the M33 disk is relatively flat (Corbelli 2003; Putman et al. 2009), in agreement with the Martinez-Serrano et al. (2009) models. The general trend of increasing specific SFR with radius in the main body of the disk predicted by the models is also consistent with the relative contributions made by young and old stars shown in Figure 15. Still, the muted evidence for star formation outside of the break radius in M33 is not consistent with the models, and the presence of tidal features in the HI distribution outside of the disk (Putman et al. 2009) points to an event that undoubtedly affected the evolution of M33. The presence of large-scale tidal features aside, the distributions of gas and stars within the break radius of M33, where the characteristic timescale for relaxation is shorter than at large radii, are at least qualitatively consistent with predictions made for disk galaxies evolving in the CDM cosmological paradigm. That the relative distributions of gas and stars in the main disk of M33 are consistent with that of an isolated disk suggests that sufficient time has passed (i.e. a few disk rotations) to allow the distributions of stars and gas within the disk to regain at least the semblance of an equilibrium state.

7.3. The M31-M33 Connection

An interaction between M31 and M33 would almost certainly have imprinted signatures in the stellar content of the former. McConnachie et al. (2009) suggest that an interaction with M33 would have disturbed the outer disk of M31, causing a warp and displacing disk stars to large radii. An interaction with M33 may also have triggered an inward flow of

gas in M31, depleting gas reserves at large radii. Indeed, the gas content of M31 at large radii is deficient when compared with models of isolated evolution (Yin et al. 2009). The interaction may also have produced elevated SFRs in M31, and a sharp drop in overall star-forming activity would occur as gas is consumed during star formation or is disrupted by feedback. Williams (2002) concludes that a global downturn in star-forming activity occurred in M31 ~ 1 Gyr in the past. Given that starbursts appear to last no more than a Gyr (e.g. Leitherer 2001), then this result – if due to an interaction with M33 – suggests that M31 and M33 interacted no more than ~ 2 Gyr ago, which is consistent with the age ranges estimated by Putman et al. (2009) and McConnachie et al. (2009). Of course, all of these properties of M31 could also be explained by an interaction with another (possibly now defunct) companion.

If there was a close interaction between M31 and M33 then some of the features traditionally associated with M31 companions could instead be remnants of this interaction. Consider the M31 Giant Southern Stream (GSS; Ibata et al. 2001). The simulations run by Bekki (2008) indicate that M33 may leave a gaseous debris stream near M31, and Fardal et al. (2008) conclude that the GSS may have originated from a spiral galaxy. Indeed, the GSS contains stars with a metallicity as high as $[\text{Fe}/\text{H}] \sim -0.5$ (Guhathakurta et al. 2006), which is consistent with an origin in the M33 disk. The velocity dispersion of stars in the GSS (e.g. Ibata et al. 2004) is also consistent with an origin in a kinematically cold environment, such as a disk. Finally, the GSS is 85 kpc behind M31 (e.g. Tanaka et al. 2010), and simulations suggest that the GSS was produced by an object on a highly eccentric orbit (Font et al. 2006; Fardal et al. 2006; 2007), such as M33.

While some properties of the GSS can be rationalized in the context of an interaction with M33, efforts to link the GSS with such an event run into timing issues. The GSS has a dynamical age of a few hundred Myr (e.g. Font et al. 2006), which is more recent than the minimum probable age for an interaction estimated by Putman et al. (2009), and is not consistent with the time interval during which there has been a constant SFR throughout the M33 disk. Another issue is that the vast majority of stars in the GSS have an age ≥ 4 Gyr (Brown et al. 2006), and so fall outside of the nominal age range predicted for an interaction. Still, a modest population of young stars is present in the GSS (e.g. Figure 17 of Brown et al. 2006). Recently formed stars in extraplanar environments may not be well-mixed with underlying stellar material, as they formed in gas concentrations, whereas pre-existing stars will tend to dissipate spatially. If this is the case in M31 then future observations may find concentrations of intermediate age stars in different fields than those sampled by Brown et al. (2006).

Program ID	u^*	g'
2003BF15	715153–156	714745 715150, 797, 935, 938 716134 718659, 894 719309, 585 724409 727548
2004BH06	774552 774554–557	
2004BH20		757867, 868 762372, 373, 374, 378, 380, 381, 382, 466–472
2004BF26		759110 761403, 560 765027, 128, 927 767646, 804, 809, 810, 975 769086, 541 773381

Table 1: Archival Data Used to Construct the Center Field Images

REFERENCES

- Barker, M. K., & Sarajedini, A. 2008, MNRAS, 390, 863
- Barnes, J. E., & Hernquist, L. 1992, Nature, 360, 715
- Bekki, K. 2008, MNRAS, 390, L24
- Bekki, K. 2009, MNRAS, 399, 2221
- Bellazzini, M., Cacciari, C., Federici, L., Fusi Pecci, F., & Rich, R. M. 2003, A&A, 405, 867
- Blitz, L., & Rosolowsky, E. 2006, ApJ, 650, 933
- Block, D. L., et al. 2006, Nature, 443, 832
- Block, D. L., et al. 2007, A&A, 471, 467
- Bonanos, A. Z., et al. 2006, ApJ, 652, 313
- Boulade, O., et al. 2003, Proc. SPIE, 4841, 72
- Bournaud, F., & Duc, P.-A. 2006, A&A, 456, 481
- Braun, R., & Thilker, D. A. 2004, A&A, 417, 421
- Brown, T. M., et al. 2006, ApJ, 652, 323
- Bush, S. J., Cox, T. J., Hayward, C. C., Thilker, D., Hernquist, L., & Besla, G. 2010, ApJ, 713, 780
- Chandar, R., Bianchi, L., & Ford, H. C. 1999, ApJ, 517, 668
- Cignoni, M., et al. 2009, AJ, 137, 3668
- Cioni, M.-R. L. 2009, A&A, 506, 1137
- Cioni, M.-R. L., et al. 2008, A&A, 487, 131
- Colavitti, E., Cescutti, G., Matteucci, F., & Murante, G. 2009, A&A, 496, 429
- Corbelli, E. 2003, MNRAS, 342, 199
- Davidge, T. J. 2000, AJ, 119, 748
- Davidge, T. J., & Courteau, S. 2002, AJ, 123, 1438
- Davidge, T. J. 2003, AJ, 125, 3046
- Davidge, T. J. 2007, ApJ, 664, 820
- Davidge, T. J. 2008, PASP, 120, 1145
- Davidge, T. J. 2010, ApJ, 725, 1342
- Davidge, T. J., Puzia, T. H., & McConnachie, A. 2011, ApJ, 728, L23

- de Jong, R. S., et al. 2007, *ApJ*, 667, L49
- de Mello, D. F., Smith, L. J., Sabbi, E., Gallagher, J. S., Mountain, M., & Harbeck, D. R. 2008, *AJ*, 135, 548
- Efremov, Y. N. 1995, *AJ*, 110, 2757
- Elmegreen, B. G., Elmegreen, D. M., & Leitner, S. N. 2003, *ApJ*, 590, 271
- Fardal, M. A., Babul, A., Guhathakurta, P., Gilbert, K. M., & Dodge, C. 2008, *ApJ*, 682, L33
- Font, A., S., Johnston, K. V., Guhathakurta, P., Majewski, S., R., & Rich, R. M. 2006, *AJ*, 131, 1436
- Forbes, D. A., & Bridges, T. 2010, *MNRAS*, 404, 1203
- Galleti, S., Bellazzini, M., & Ferraro, F. R. 2004, *A&A*, 423, 925
- Girardi, L., Grebel, E. K., Odenkirchen, M., & Chiosi, C. 2004, *A&A*, 422, 205
- Gogarten, S. M., et al. (2010), *ApJ*, 712, 858
- Guhathakurta, P., et al. 2006, *AJ*, 131, 2497
- Hammer, F., Puech, M., Chemin, L., Flores, H., & Lehnert, M. 2007, *ApJ*, 662, 322
- Harris, J., & Zaritsky, D. 2001, *ApJS*, 136, 25
- Helmi, A., Navarro, J. F., Nordstrom, B., Holmberg, J., Abadi, M. G., & Steinmetz, M. 2006, *MNRAS*, 365, 1309
- Herrmann, K. A., Ciardullo, R., & Sigurdsson, S. 2009, *ApJ*, 693, L19
- Humphreys, R. M., & Sandage, A. 1980, *ApJS*, 44, 319
- Ibata, R. A., Gilmore, G., & Irwin, M. J. 1994, *Nature*, 370, 6486
- Ibata, R., Irwin, M., Lewis, G., Ferguson, A. M. N., & Tanvir, N. 2001, *Nature*, 412, 49
- Ibata, R., Chapman, S., Ferguson, A. M. N., Irwin, M., Lewis, G., & McConnachie, A. 2004, *MNRAS*, 351, 117
- Ibata, R., Martin, N. F., Irwin, M., Chapman, S., Ferguson, A. M. N., Lewis, G. F., & McConnachie, A. W. 2007, *ApJ*, 671, 1591
- Inoue, A. K., Hirashita, H., & Kamaya, H. 2000, *AJ*, 120, 2415
- Johnston, K. V., Hernquist, L., & Bolte, M. 1996, *ApJ*, 465, 278
- Kroupa, P., Tout, C. A., & Gilmore, G. 1993, *MNRAS*, 262, 545
- Kroupa, P. 2001, *MNRAS*, 322, 231

- Leitherer, C. 2001, in *Astrophysical Ages and Time Scales*, ASP Conference 245, ed. T. von Hippel, C. Simpson, & N. Manset, pp. 390
- Li, J., Ma, J., Xhou, X., Jiang, Z., Yang, Y., & Chen, J. 2004, *A&A*, 420, 89
- Magrini, L., Stanghellini, L., & Villaver, E. 2009, *ApJ*, 696, 729
- Magrini, L., Stanghellini, L., Corbelli, E., Galli, D., & Villaver, E. 2010, *A&A*, 512, 63
- Martin, C. L., & Kennicutt, R. C. Jr. 2001, *ApJ*, 555, 301
- Martinez-Serrano, F. J., Serna, A., Domenech-Moral, M., & Dominguez-Tenreiro, R. 2009, *ApJ*, 705, L133
- Massey, P., Olsen, K. A. G., Hodge, P. W., Strong, S. B., Jacoby, G. H., Schlingman, W., & Smith, R. C. 2006, *AJ*, 131, 2478
- McConnachie, A., et al. 2009, *Nature*, 461, 66
- McConnachie, A., et al. 2010, *ApJ*, 723, 1038
- Melbourne, J., et al. 2010, *ApJ*, 712, 469
- Mouhcine, M., & Ibata, R. 2009, *MNRAS*, 399, 737
- Munoz-Mateos, J. C., Gil de Paz, A., Boissier, S., Zamorano, J., Jarrett, T., Gallego, J., & Madore, B. F. 2007, *ApJ*, 658, 1006
- Neff, S. G., et al. 2005, *ApJ*, 619, L91
- Oh, S. H., Kim, W-T, Lee, H. M., & Kim, J. 2008, *ApJ*, 683, 94
- Park, W-K, Park, H. S., & Lee, M. G. 2009, *ApJ*, 700, 103
- Pierce, M. J., & Tully, R. B. 1992, *ApJ*, 387, 47
- Putman, M. E. et al. 2009, *ApJ*, 703, 1486
- Roskar, R., Debattista, V. P., Stinson, G. S., Quinn, T. R., Kaufmann, T., & Wadsley, J. 2008, *ApJ*, 675, L65
- Rosolowsky, E., & Simon, J. D. 2008, *ApJ*, 675, 1213
- Salpeter, E. E. 1955, *ApJ*, 121, 161
- San Roman, I., Sarajedini, A., & Aparicio, A. 2010, *ApJ*, 720, 1674
- Sanchez-Blazquez, P., Courty, S., Gibson, B. K., & Brook, C. B. 2009, *MNRAS*, 398, 591
- Schlegel, D. J., Finkbeiner, D. P., & Davis, M. 1998, *ApJ*, 500, 525
- Schonrich, R., & Binney, J. 2009, *MNRAS*, 399, 1145
- Sellwood, J. A., & Binney, J. J. 2002, *MNRAS*, 336, 785

- Sheth, K., Vogel, S. N., Wilson, C. D., & Dame, T. M. 2008, *ApJ*, 675, 330
- Smith, J. A., et al. 2002, *AJ*, 123, 2121
- Stetson, P. B. 1987, *PASP*, 99, 191
- Stetson, P. B., & Harris, W. E. 1988, *AJ*, 96, 909
- Tanaka, M., Chiba, M., Komiyama, Y., Guhathakurta, P., Kalirai, J. S., & Iye, M. 2010, *ApJ*, 708, 1168
- Teyssier, M., Johnston, K. V., & Shara, M. M. 2009, *ApJ*, 707, L22
- Thilker, D. A., et al. 2005a, *ApJ*, 619, L67
- Thilker, D. A., et al. 2005b, *ApJ*, 619, L79
- U, V., Urbaneja, M. A., Kudritzky, R-P, Jacobs, B. A., Bresolin, F., & Przybilla, N. 2009, *ApJ*, 704, 1120
- Verley, S., Corbelli, E., Giovanardi, C., & Hunt, L. K. 2009, *A&A*, 493, 453
- Verley, S., Corbelli, E., Giovanardi, C., & Hunt, L. K. 2010, *A&A*, 510, 64
- Williams, B. F. 2002, *MNRAS*, 331, 293
- Williams, B. F., Dalcanton, J. J., Dolphin, A. E., Holtzman, J., & Sarajedini, A. 2009, *ApJ*, 695, L15
- Yin, J., Hou, J. L., Prantzos, N., Boissier, S., Chang, R. X., Shen, S. Y., & Zhang, B. 2009, *A&A*, 505, 497
- Younger, J. D., Cox, T. J., Seth, A. C., & Hernquist, L. 2007, *ApJ*, 670, 269
- Yun, M. S., Ho, P. T. P., & Lo, K. Y. 1994, *Nature*, 372, 530
- Zaritsky, D., & Christlein, D. 2007, *AJ*, 134, 135
- Zaritsky, D., Kennicutt, R. C. Jr., & Huchra, J. P. 1994, *ApJ*, 420, 87

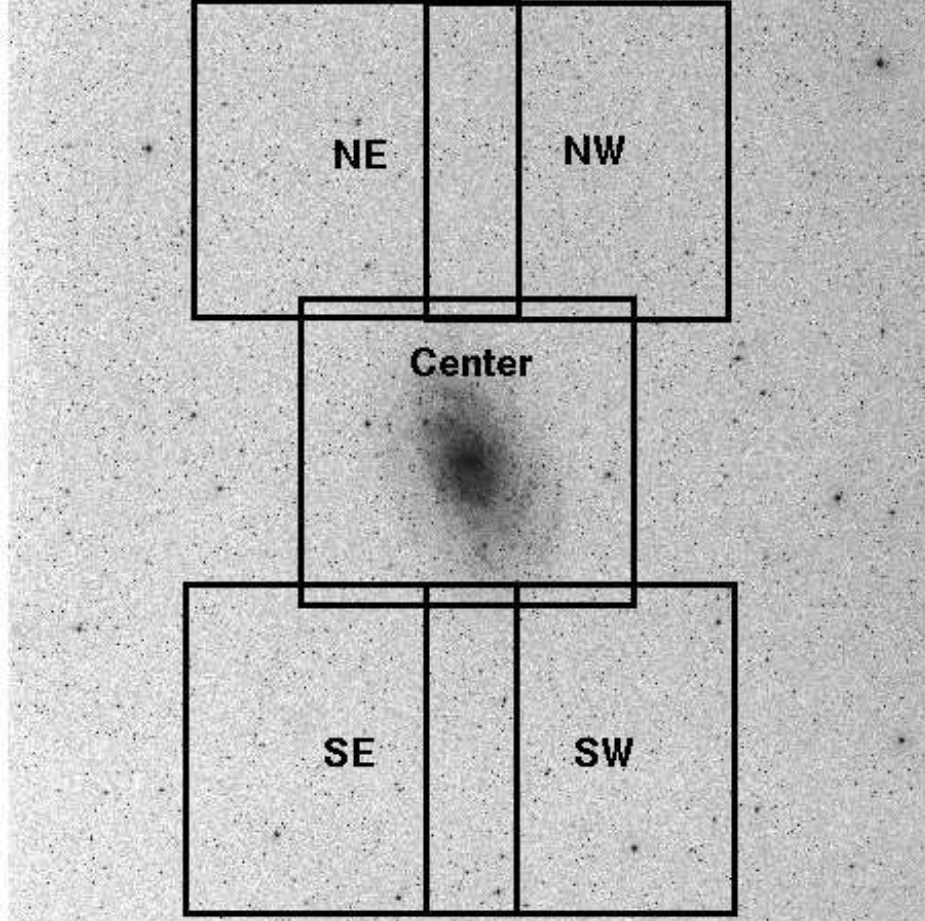


Fig. 1.— The locations of the fields discussed in this paper. The underlying reference image is from the DSS in the blue filter. East is to the left and north at the top. Each MegaCam field covers roughly 1 degree^2 , and is labelled with the identifier that is used throughout the paper.

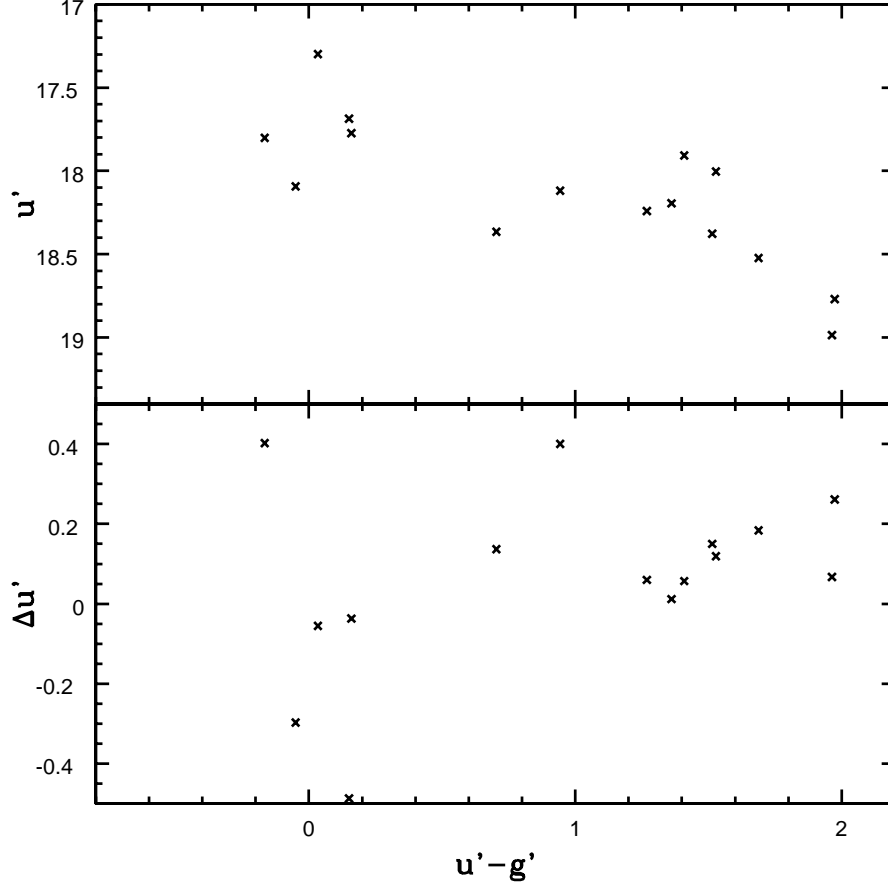


Fig. 2.— (Top panel:) The CMD of bright, isolated sources that are also in the sample observed by Massey et al. (2006). The majority of objects in both samples have red colors, and this is because the crowded regions of the disk, where bright blue stars are located, were intentionally avoided when comparing the two sets of measurements. (Lower panel:) The difference between the MegaCam and NOAO measurements, $\Delta u'$, with respect to $u' - g'$. The Spearman correlation coefficient indicates that $\Delta u'$ does not vary in a systematic way with color. With the exception of the four outliers, the majority of points have ± 0.1 magnitude scatter in $\Delta u'$, which is comparable to the dispersion about the empirical relation between $u' - g'$ and $U - B$ in Figure 13 of Smith et al. (2002).

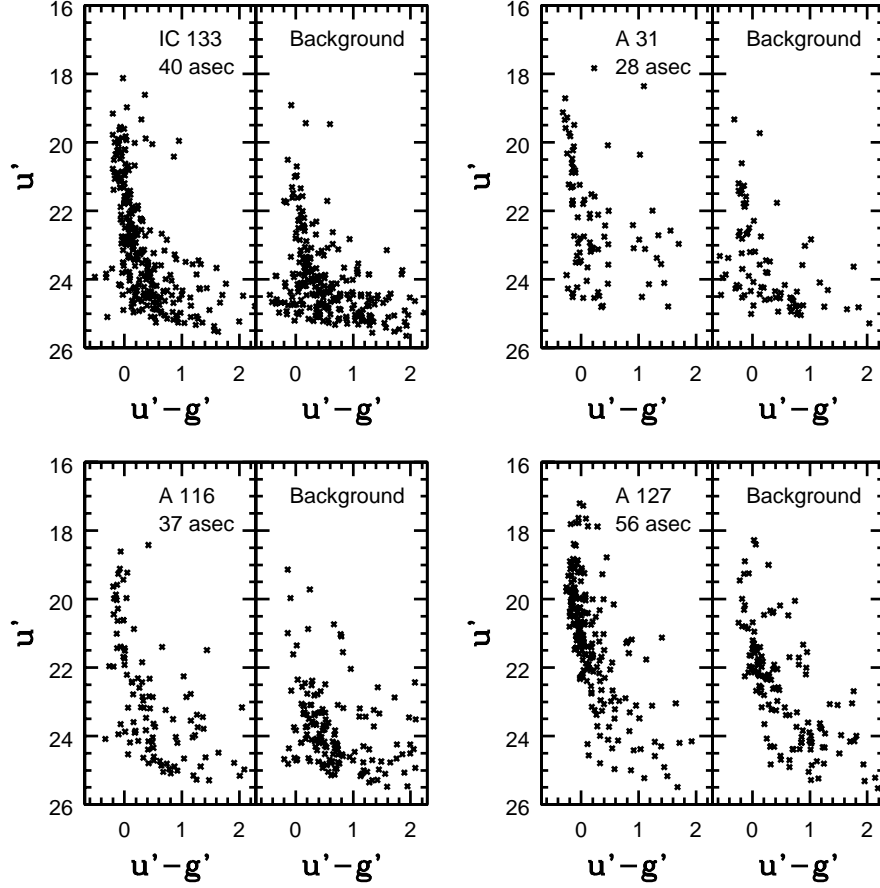


Fig. 3.— The $(u', u' - g')$ CMDs of four star-forming complexes that are located in low-density regions of the M33 disk. The approximate radial size of each cluster is specified. The CMDs of sources in an annulus that surrounds each cluster are also shown; this annulus samples the same total area on the sky as the cluster that it abuts. The main sequence is clearly seen in each CMD, and sources to the right of the main sequence are BSGs. The CMDs of IC 133, A 31, and A 116 are well-populated down to $u' = 24 - 25$. However, the number counts in the A 127 CMD drop when $u' > 22$. This drop is probably due to crowding, as A 127 is the structure with the highest mean surface brightness. The objects with $u' > 22$ in the A 127 CMD are located in lower density parts of this complex.

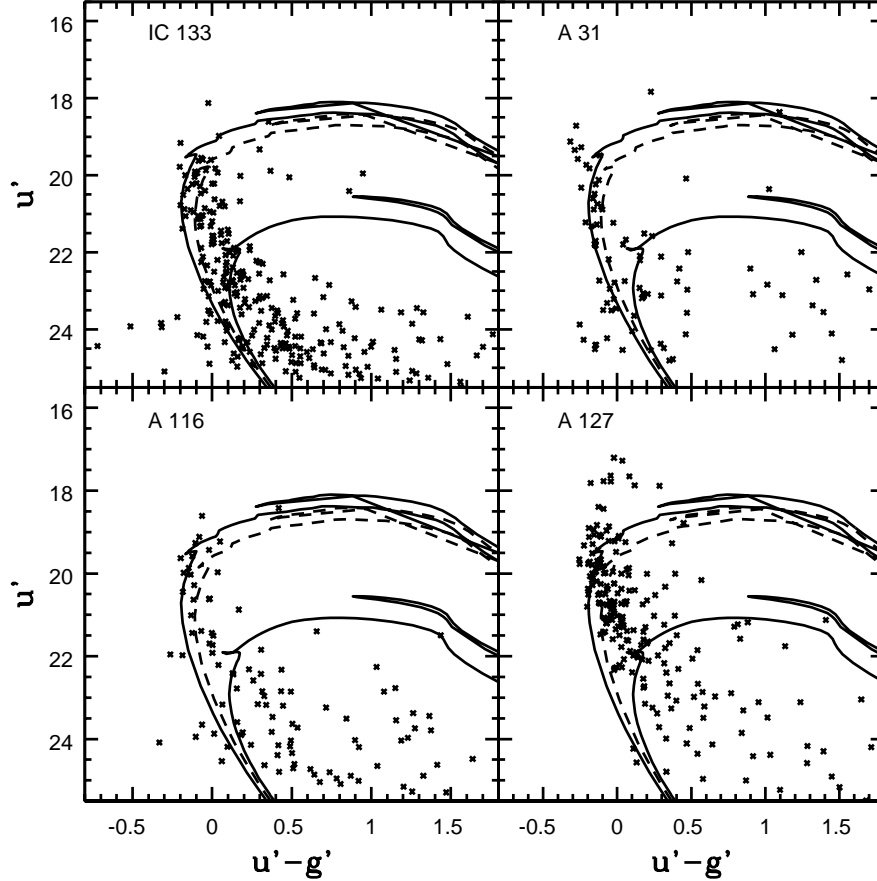


Fig. 4.— The $(u', u' - g')$ CMDs of four star-forming complexes are compared with isochrones from Girardi et al. (2004). The models have $Z = 0.008$ and ages 10 Myr and 40 Myr. The isochrones plotted as solid lines assume a combined foreground and internal extinction $A_B = 0.34$ magnitudes, which is the default reddening used throughout this study (§1). The dashed line shows the 10 Myr isochrone with an additional extinction $A_V = 0.2$ mag. The CMD of A 31 is well matched by the 10 Myr isochrones down to $u' \sim 24$, whereas the CMD of A 116 follows the 10 Myr isochrone when $u' < 22$. However, the agreement with the isochrones is not as good for IC 133 and A 127. In the case of IC 133 the morphology of the CMD suggests that this structure might contain stars that formed within the past ~ 100 Myr, which is the approximate lifetime for large star-forming complexes (e.g. Davidge et al. 2011). The agreement with the models is poorest for A 127.

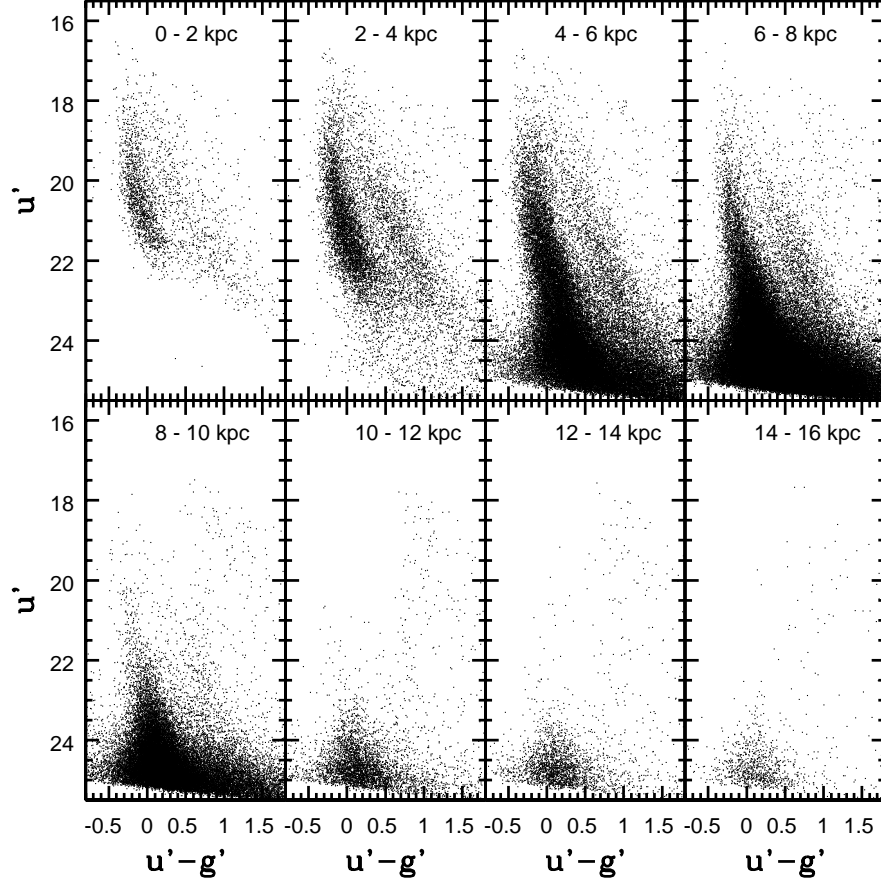


Fig. 5.— The $(u', u' - g')$ CMDs of stars in the disk of M33. A bright main sequence dominates the CMDs with $R_{GC} \leq 10$ kpc, and the peak brightness of the bluest objects is roughly constant when $R_{GC} \leq 8$ kpc. BSGs form a distinct spray of stars to the right of the main sequence. The plume of objects with $u' - g'$ between 1.0 and 1.5 in the CMDs with $R_{GC} \geq 8$ kpc is populated by background galaxies.

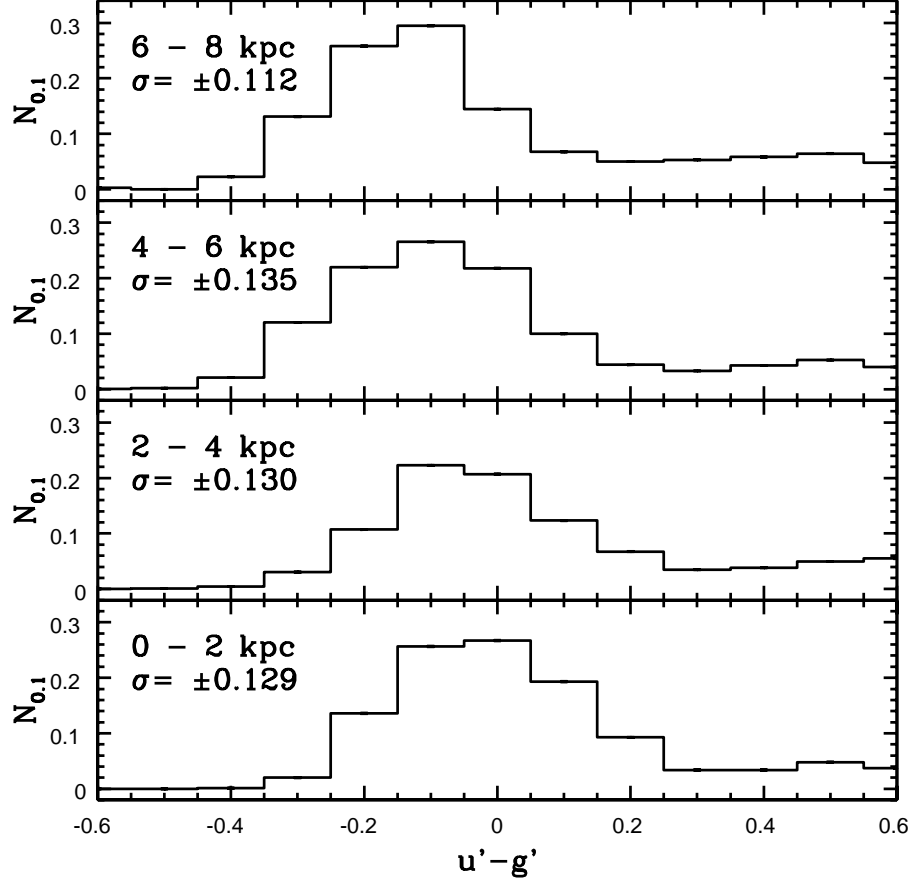


Fig. 6.— The $u' - g'$ distributions of stars with u' between 20.5 and 21.5. The prominent peak in each color distribution is due to main sequence stars, while the tail to the right of this peak is made up of stars that have evolved off the main sequence. The distributions have been normalized according to the number of objects with $u - g'$ between -0.35 and 0.35 ; σ is the standard deviation of each distribution. There is a trend towards bluer mean $u' - g'$ colors in the main sequence as R_{GC} increases. If the SFH in the past few tens of Myr has not changed, as suggested by the investigation of main sequence LFs in §5, then this color trend may be indicative of higher levels of internal extinction at smaller R_{GC} , such that $\Delta A_V / \Delta R_{GC} = -0.05 \text{ mag kpc}^{-1}$. The $u' - g'$ distributions of main sequence stars are wider than predicted from random photometric errors, and the excess width suggests that differential reddening within the inner disk of M33 introduces a dispersion $\Delta E(B - V) \leq \pm 0.10 \text{ mag}$.

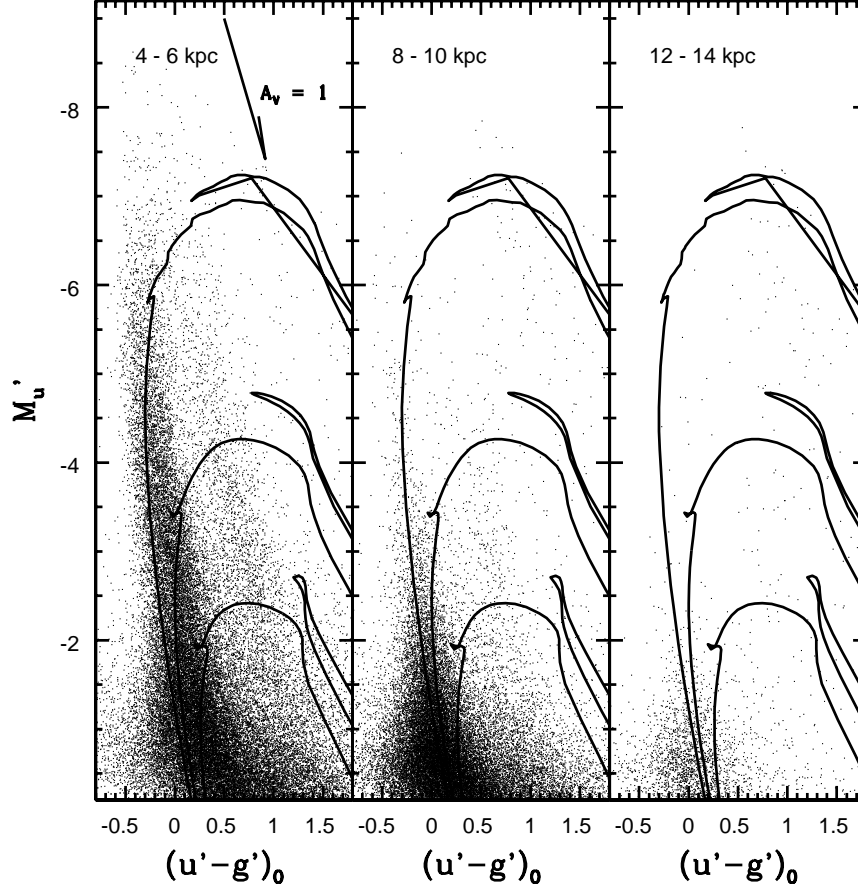


Fig. 7.— The $(M_{u'}, u' - g')$ CMDs of sources in three annuli. Also shown are $Z = 0.008$ isochrones from Girardi et al. (2004) with ages 10 Myr, 40 Myr, and 100 Myr. There is reasonable agreement between the isochrones and the observed locus of main sequence stars, lending credence to the baseline reddening value. A reddening vector with a length that corresponds to $A_V = 1$ mag is shown in the 4 – 6 kpc panel.

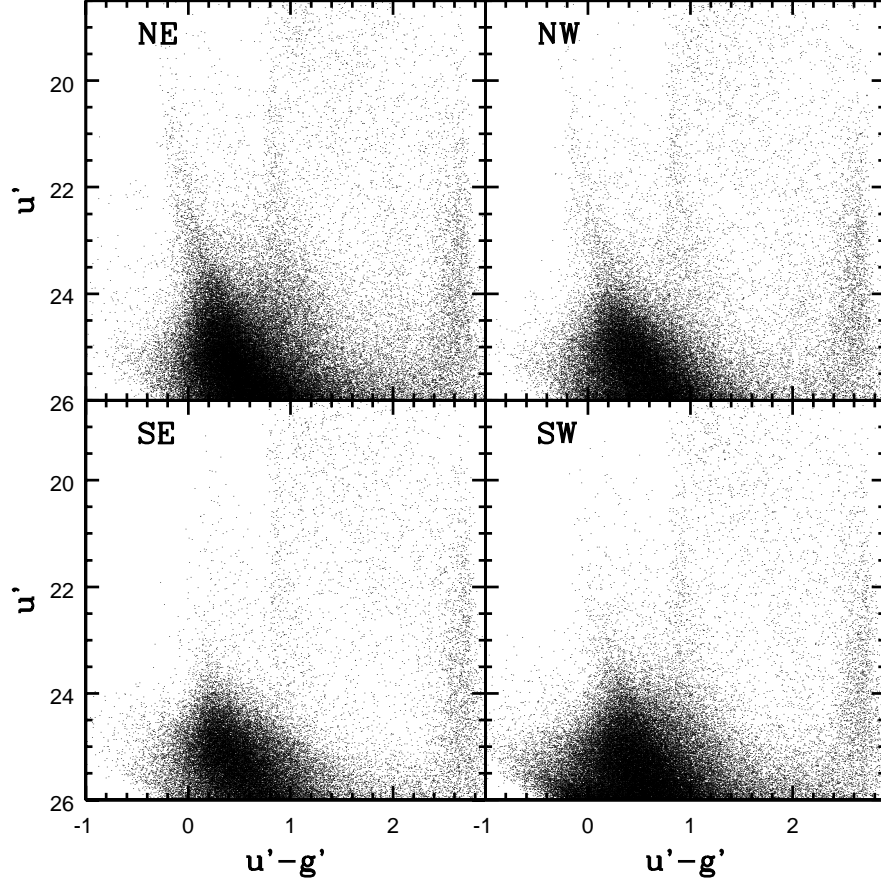


Fig. 8.— The $(u', u' - g')$ CMD of sources in the NE, NW, SE, and SW fields. The bright blue plume in the NE and NW CMDs is populated by massive main sequence stars that are near the edge of the northern spiral arm. A less well-populated main sequence is seen in the CMD of the SW field. The majority of sources with $u' - g' > 1$ and $u' > 24$ are background galaxies, although the evolutionary tracks of intermediate age He-burning stars also pass through this part of the CMD.

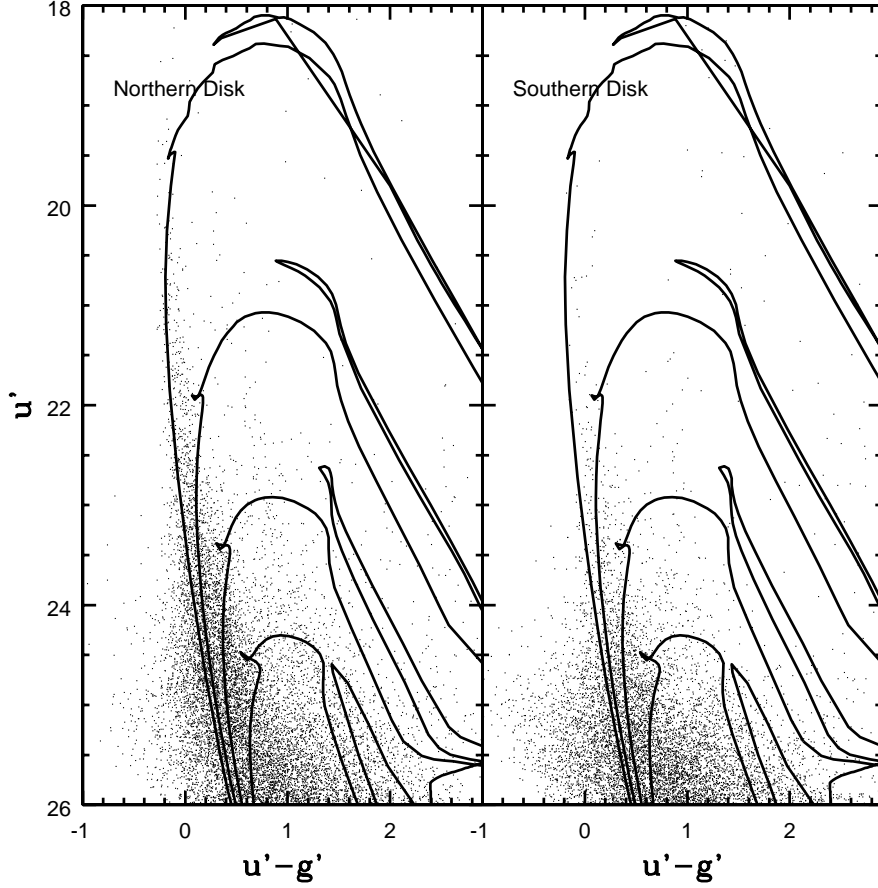


Fig. 9.— The $(u', u' - g')$ CMD of sources at the periphery of the M33 disk, in the areas indicated in Figure 17. The CMDs are compared with $Z=0.008$ isochrones from Girardi et al. (2004) that have ages 10 Myr, 40 Myr, 100 Myr, and 200 Myr. The blue envelope of upper main sequence stars in the northern disk follows the 10 Myr isochrone, and the observed main sequence width matches that predicted by the models. In contrast to the Northern Disk, only a handful of stars in the Southern Disk formed within the past few tens of 10 Myr.

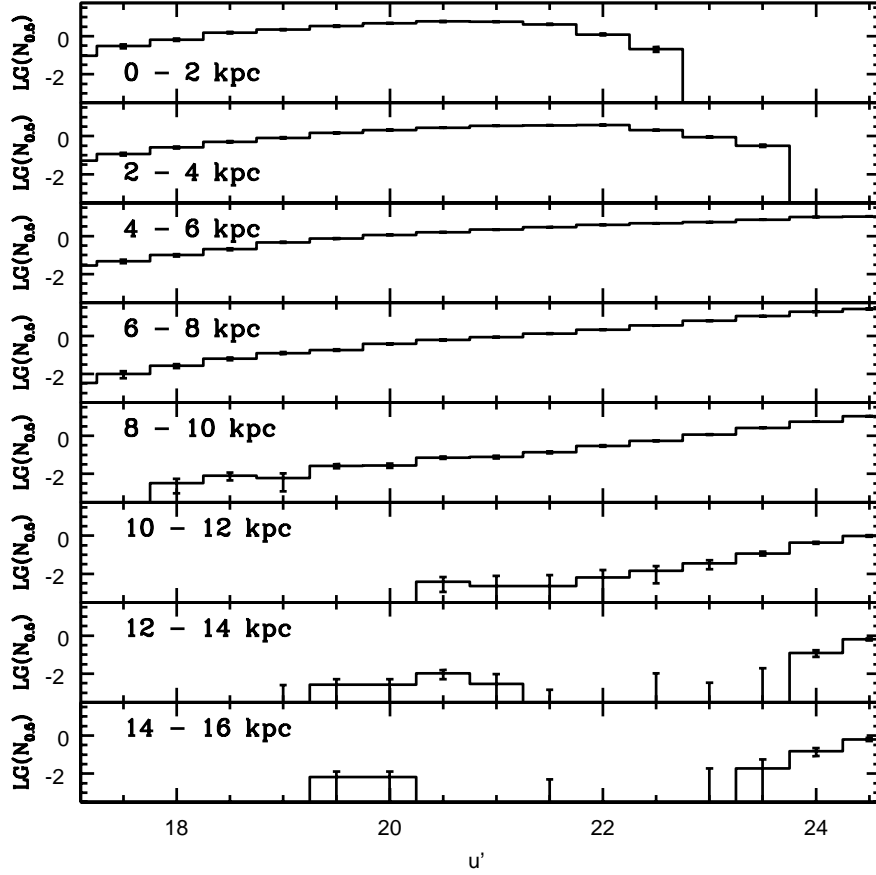


Fig. 10.— The LFs of main sequence stars in the Center Field. Distances are measured in the plane of the M33 disk, and $N_{0.5}$ is the number of sources arcmin^{-2} per 0.5 magnitude interval in u' , corrected for foreground star/background galaxy contamination using source counts from the outermost parts of the NE field. Crowding elevates the faint limit in the 0 - 2 and 2 - 4 kpc intervals when compared with larger R_{GC} . The shape of the LFs changes near 8 kpc. The LFs with $R_{GC} \leq 8$ kpc follow power laws that can be characterized by a single exponent. In contrast, at larger radii the bright end of the LF flattens while the faint end steepens. The peak brightness of the main sequence also drops with increasing R_{GC} when $R_{GC} \geq 8$ kpc. These results are consistent with previous studies that have found that the distribution of young stars in M33 changes near $R_{GC} = 8$ kpc.

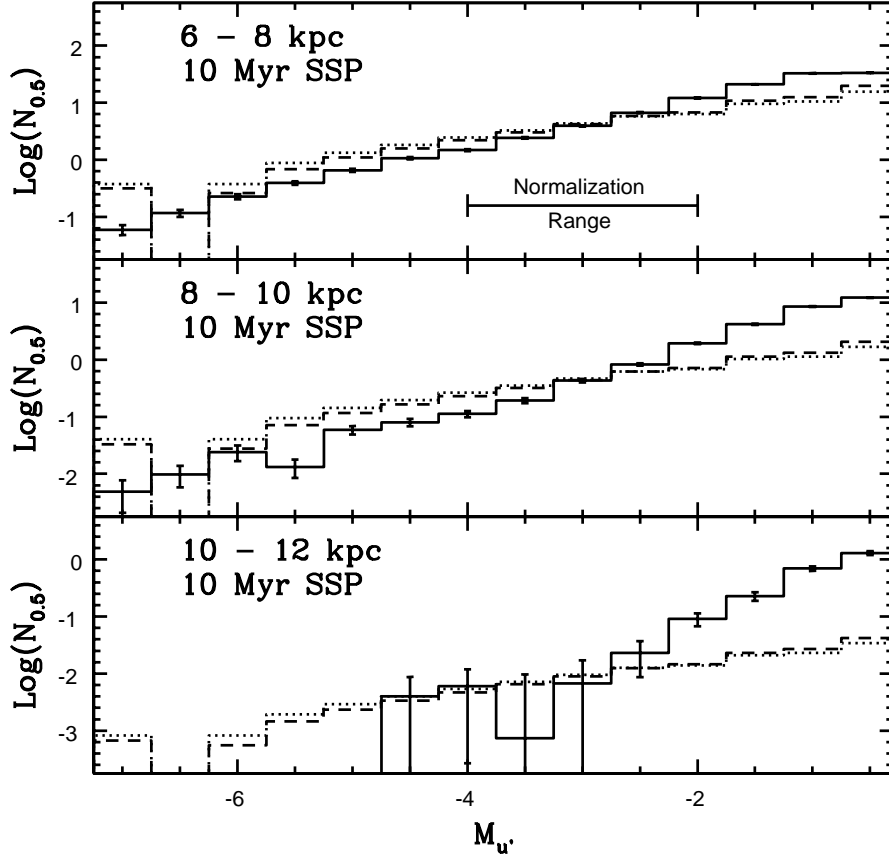


Fig. 11.— Simple stellar population (SSP) model LFs with Salpeter (dotted line) and Kroupa (dashed line) IMFs are compared with observed LFs. The models are normalized to match the observations in the interval $M_{u'} = -2$ to -4 . $N_{0.5}$ is the number of sources arcmin^{-2} per 0.5 magnitude interval in u' . The SSP model LFs are significantly flatter than the observed LFs, indicating that the youngest stars in the M33 disk did not form during a single event.

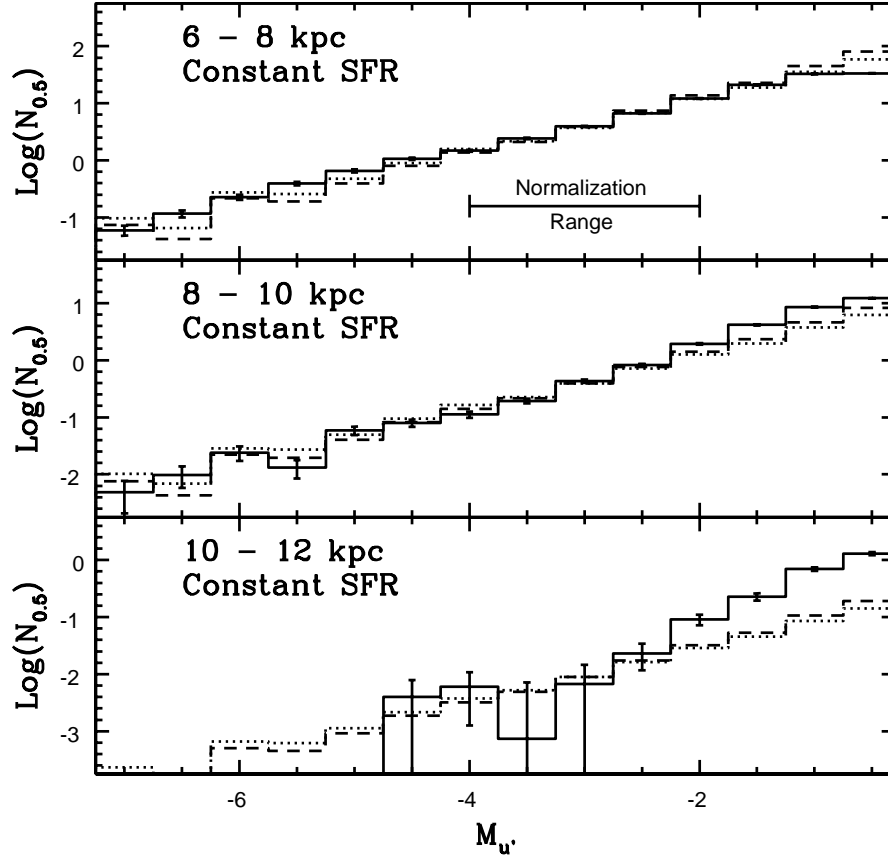


Fig. 12.— The same as Figure 11, but showing constant SFR models. These models provide a reasonable match to the 6 – 8 kpc and 8 – 10 kpc LFs over a wide range of magnitudes. However, the 10 – 12 kpc LF is steeper than predicted by the models.

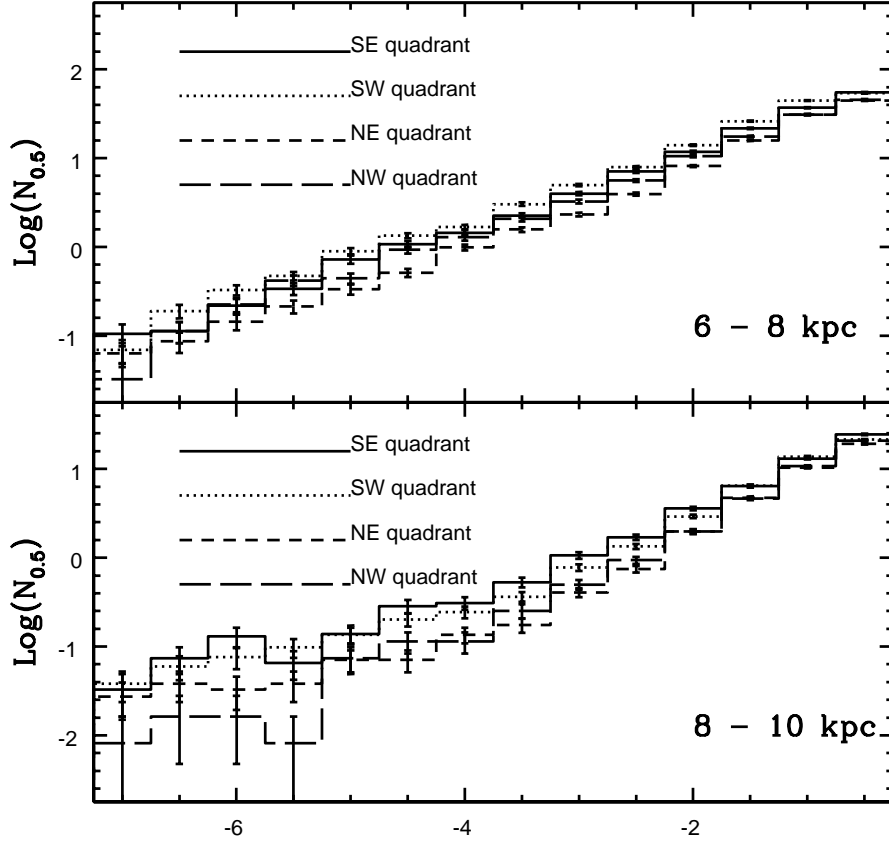


Fig. 13.— Quadrant-to-quadrant variations in the LFs of main sequence stars are examined in this figure. $N_{0.5}$ is the number of sources arcmin^{-2} per 0.5 magnitude interval in u' in each quadrant. There is a systematic tendency for the number counts in the interval $M_{u'} \leq -1$ in the southern half of the galaxy to be higher than in the northern half. This suggests that for $R_{GC} > 6$ kpc the southern half of the disk experienced a higher SFR during the past few tens of Myr than the northern half of the disk.

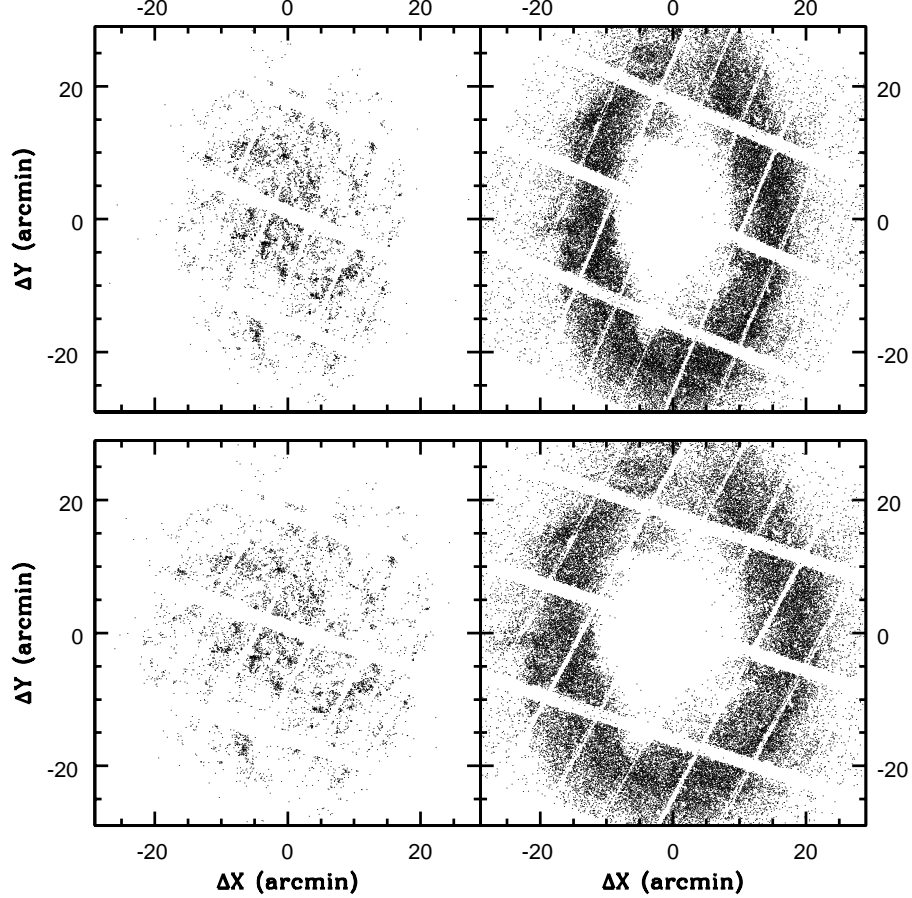


Fig. 14.— The observed (top row) and de-projected (bottom row) distributions of stars in M33. The 10 Myr and 100 Myr samples were selected based on location in the $(u', u' - g')$ CMD, as defined in Figure 1 of Davidge et al. (2011). M33 is oriented such that the major axis parallels the vertical axis. The axis labels are offsets from the center of M33 in the rotated reference frame. The spiral structure defined by the 10 Myr data can be traced into the central regions of the galaxy. With the exception of the sharp outer disk boundary, distinct structures are much less obvious in the 100 Myr sample. Crowding prevents the detection of main sequence stars with ages ~ 100 Myr in the central regions of the galaxy.

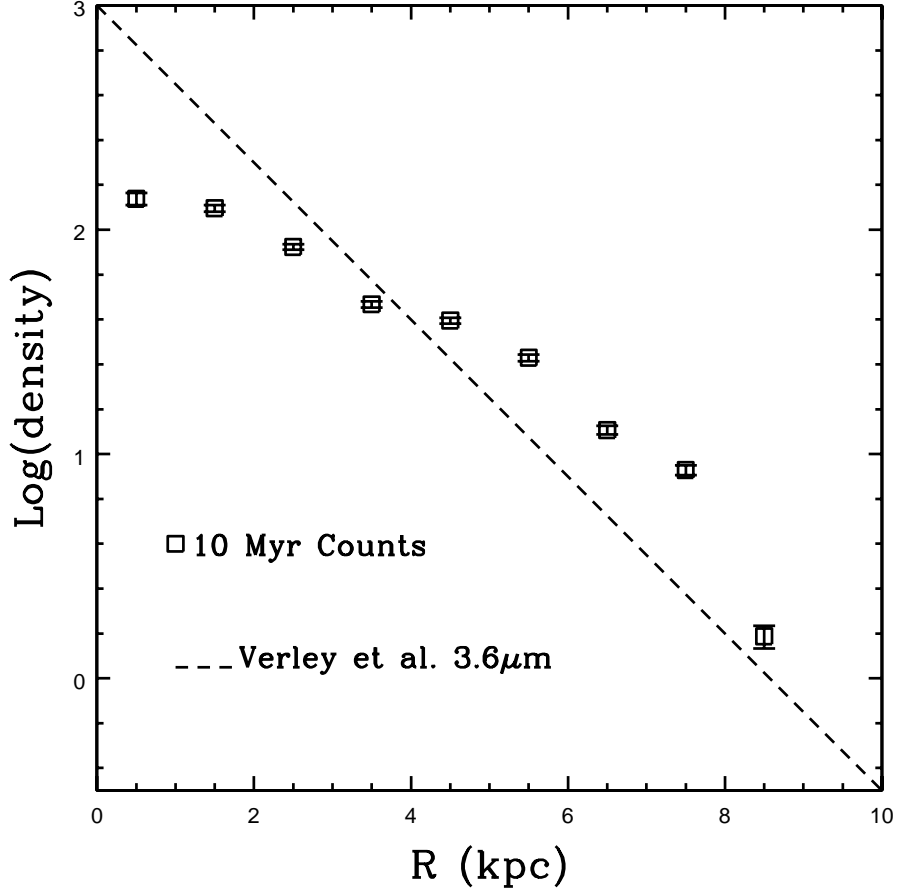


Fig. 15.— The number of 10 Myr sources kpc^{-2} is compared with the $3.6\mu\text{m}$ integrated light profile from Figure 2 of Verley et al. (2009). The slope of the $3.6\mu\text{m}$ profile has been adjusted to account for the distance modulus adopted for the present study, which differs from that assumed by Verley et al. (2009). The light at $3.6\mu\text{m}$ is dominated by old and intermediate-age stars, and so traces stellar mass. The 10 Myr number counts define a more-or-less linear relation out to $R_{GC} = 8 \text{ kpc}$ that is flatter than the $3.6\mu\text{m}$ light profile. The contribution made by young stars to the total stellar mass density thus grows with increasing R_{GC} out to 8 kpc, but then drops at larger radii.

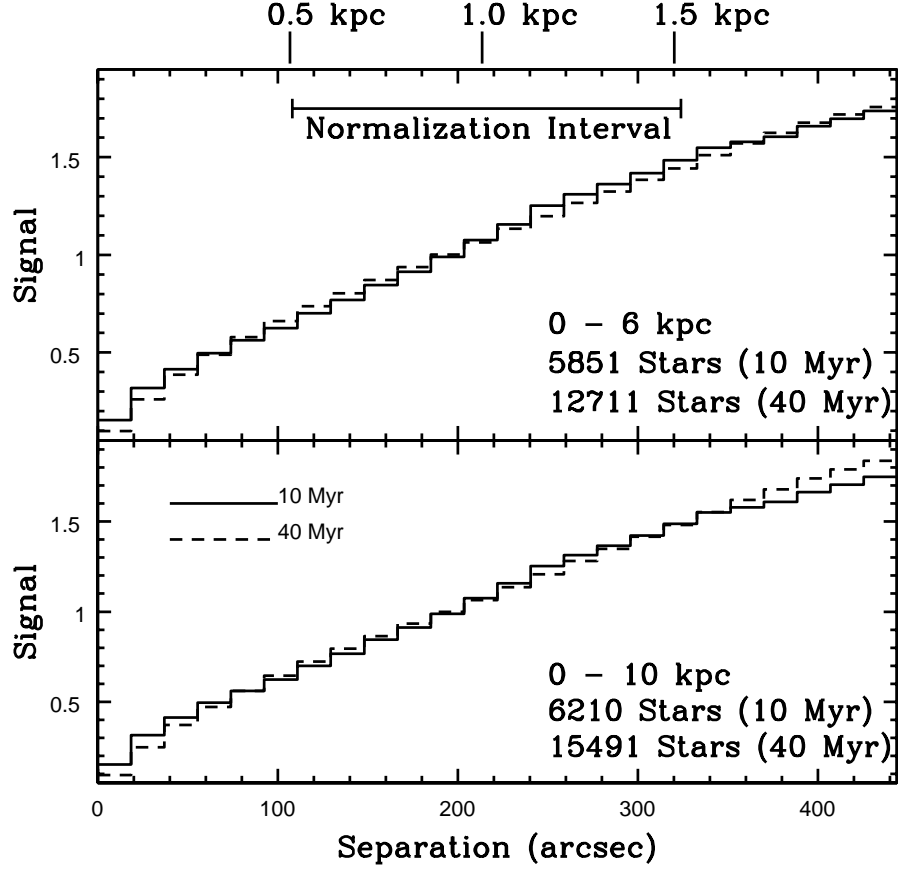


Fig. 16.— The star-star separation functions (S3Fs) of main sequence stars in the 10 and 40 Myr groups. The signals have been normalized to the numbers of sources with separations between 0.5 and 1.5 kpc (110 - 330 arcsec). At separations < 200 arcsec (< 0.9 kpc) the 40 Myr S3Fs are steeper than the 10 Myr functions. The signal at separations < 60 arcsec (< 280 parsecs) in both radial intervals of the 40 Myr S3Fs is then smaller than in the 10 Myr sample, indicating a diminished degree of grouping over these spatial scales.

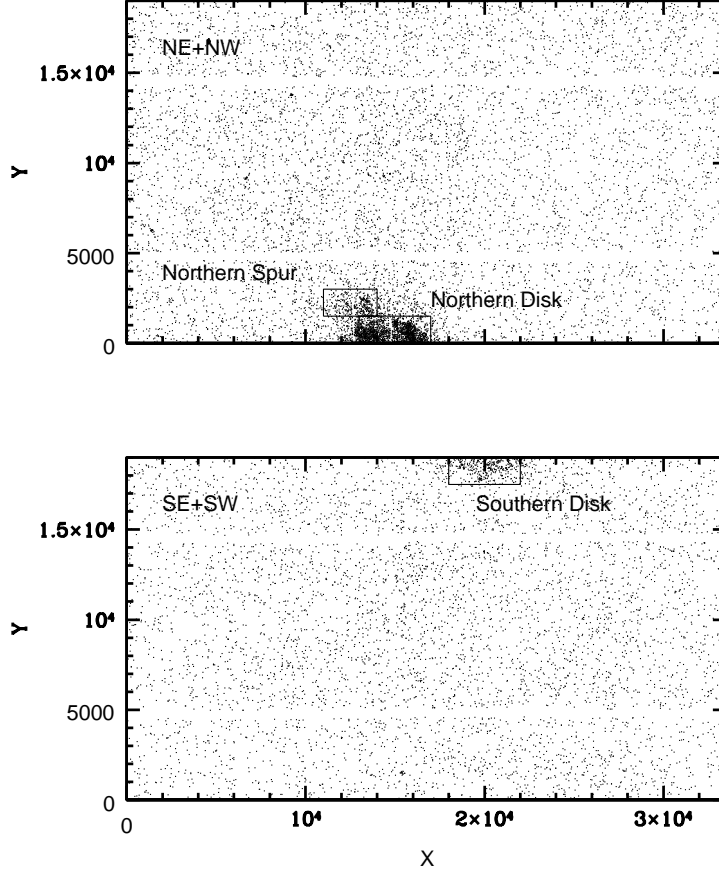


Fig. 17.— The distribution of blue sources in the NE, NW, SE, and SW fields. The objects have magnitudes and colors that place them within the 100 Myr boundaries defined in Figure 1 of Davidge et al. (2011). While having photometric properties that are consistent with those of main sequence stars, many of these sources are in fact associated with background galaxies. However, stellar concentrations near the northern and southern ends of the disk are evident, and these are indicated.

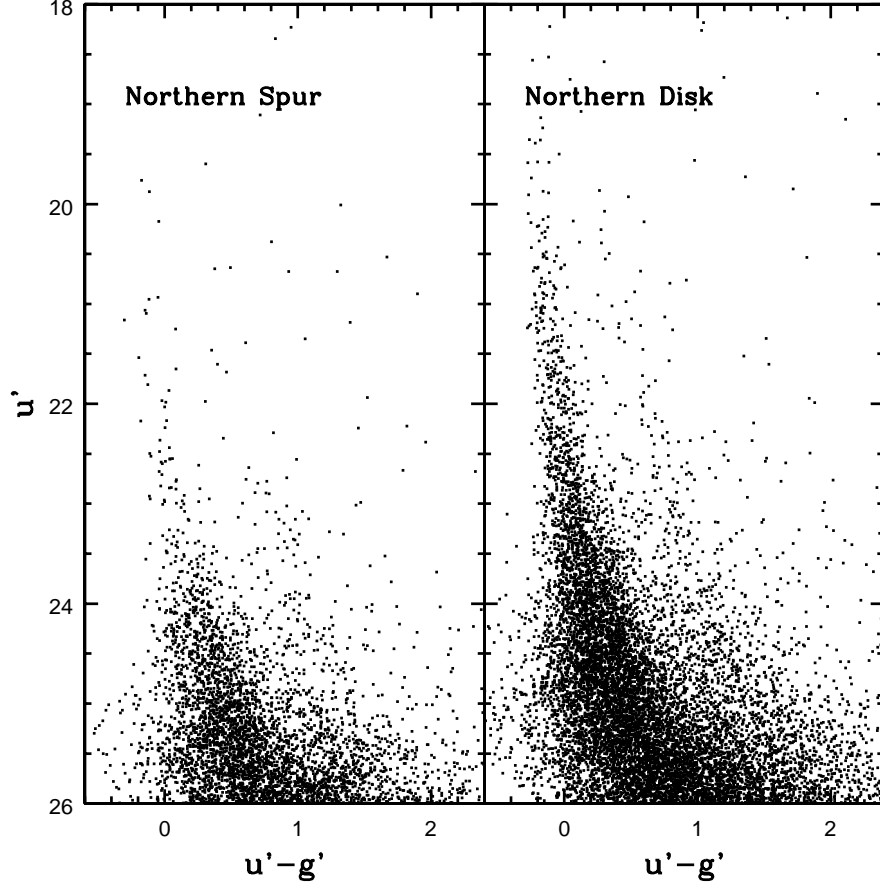


Fig. 18.— The $(u', u' - g')$ CMDs of the Northern Spur and Northern Disk. The sources used to make these CMDs fall within the areas indicated in Figure 17. The Northern Spur lacks the very bright main sequence stars that are seen in the Northern Disk. The youngest stars in the Northern Spur tend to have ages of a few tens of Myr, although the Putman et al. (2009) HI map shows that this is an area of localized HI emission.

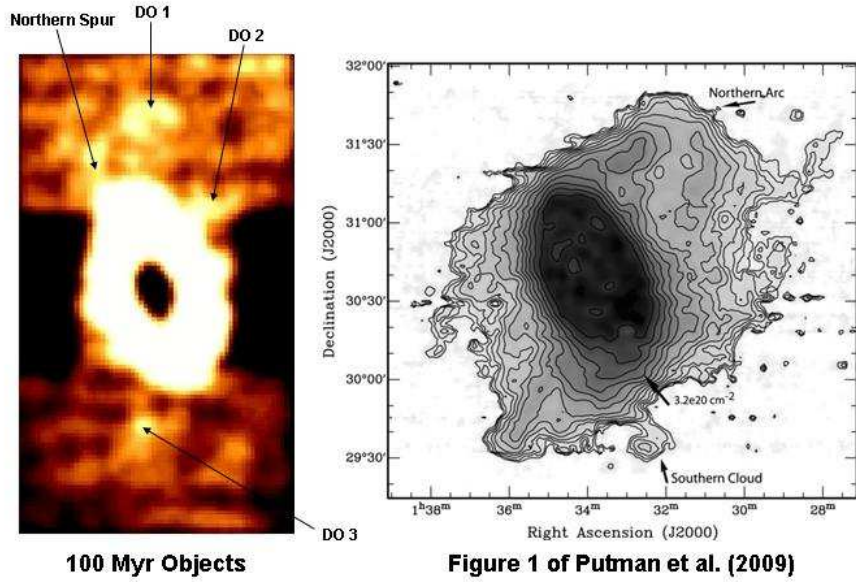


Fig. 19.— (Left hand panel) The distribution of blue sources in the MegaCam fields. An area covering $3 \times 1.7 \text{ degree}^2$ is shown, with north at the top, and east to the left. The intensity of each pixel reflects the number of sources in the 100 Myr sample in 500×500 Megacam pixel ($\sim 0.5 \times 0.5 \text{ kpc}$) gathers, after applying a low-pass filter to remove star-forming regions in background galaxies. Structures that are discussed in the text are labelled. (Right hand panel) Figure 1 of Putman et al. (2009), which shows the HI distribution in and around M33. This figure is displayed with the same spatial scale as the MegaCam image to facilitate the cross-identification of features in the HI and MegaCam data. Note that the HI contours are not smooth in the vicinity of the structures that are identified in the left hand panel.

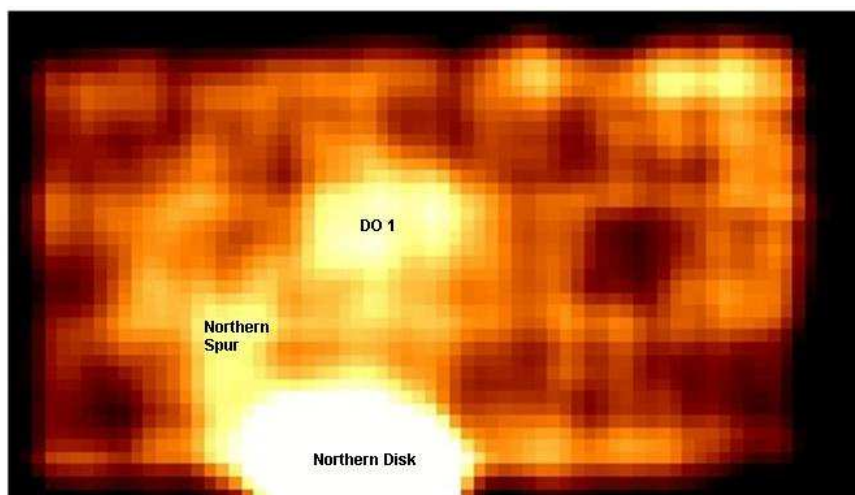


Fig. 20.— The distribution of blue sources in the NE and NW fields. A 1×1.7 degree² area is displayed, and the intensity of each pixel reflects the number of sources in the 100 Myr sample in 500×500 Megacam pixel ($\sim 0.5 \times 0.5$ kpc) gathers, after applying a low-pass filter to remove star-forming regions in background galaxies. Note that the Northern Spur is connected to the M33 disk, while a faint tongue of sources extends south of DO 1, pointing towards the M33 disk.